Science Bulletin 62 (2017) 724–740

Contents lists available at ScienceDirect

Science Bulletin

journal homepage: www.elsevier.com/locate/scib

Science Bulletin
www.scibull.com

Review

Graphene: a promising 2D material for electrochemical energy storage

Yanfeng Dong [a], Zhong-Shuai Wu [a,*], Wencai Ren [b,*], Hui-Ming Cheng [b,c], Xinhe Bao [a,d]

[a] Dalian National Laboratory for Clean Energy, Dalian Institute of Chemical Physics, Chinese Academy of Sciences, Dalian 116023, China
[b] Shenyang National Laboratory for Materials Science, Institute of Metal Research, Chinese Academy of Sciences, Shenyang 110016, China
[c] Tsinghua-Berkeley Shenzhen Institute (TBSI), Tsinghua University, Shenzhen 518055, China
[d] State Key Laboratory of Catalysis, Dalian Institute of Chemical Physics, Chinese Academy of Sciences, Dalian 116023, China

ARTICLE INFO

Article history:
Received 3 March 2017
Received in revised form 30 March 2017
Accepted 10 April 2017
Available online 19 April 2017

Keywords:
Graphene
Energy storage
Lithium ion batteries
Supercapacitors
Micro-supercapacitors
Metal air batteries
Lithium-sulfur batteries

ABSTRACT

Graphene, with unique two-dimensional form and numerous appealing properties, promises to remarkably increase the energy density and power density of electrochemical energy storage devices (EESDs), ranging from the popular lithium ion batteries and supercapacitors to next-generation high-energy batteries. Here, we review the recent advances of the state-of-the-art graphene-based materials for EESDs, including lithium ion batteries, supercapacitors, micro-supercapacitors, high-energy lithium-air and lithium-sulfur batteries, and discuss the importance of the pore, doping, assembly, hybridization and functionalization of different nano-architectures in improving electrochemical performance. The major roles of graphene are highlighted as (1) a superior active material, (2) ultrathin 2D flexible support, and (3) an inactive yet electrically conductive additive. Furthermore, we address the enormous potential of graphene for constructing new-concept emerging graphene-enabled EESDs with multiple functionalities of lightweight, ultra-flexibility, thinness, and novel cell configurations. Finally, future perspectives and challenges of graphene-based EESDs are briefly discussed.

1. Introduction

Huge depletion of fossil fuels undoubtedly intensifies the energy crisis and further deteriorates environmental issues. Electrochemical energy storage devices (EESDs) could efficiently store excess fossil energy (e.g., in power plants) or renewable energy (e.g., wind, tide and solar radiation) and provide clean energy upon working. The optimized electrodes with suitable surface area, conductivity, composition for EESDs need a systematic approach to gain the maximum efficiency [1,2], however, the existing materials could not simultaneously meet stringent requirements, such as lightweight, high conductivity, high specific surface area (SSA), tunable surface wettability, and excellent electrochemical properties. Therefore, great efforts have been made on seeking and designing novel electrode materials and their nanostructures for EESDs.

Graphene, one-atom-thick two-dimensional layer of sp^2-bonded carbon, has become one of the most important topics in the multiple fields such as materials science and condensed-matter physics [3,4]. In particular, motivated by its high theoretical SSA (2,620 $m^2 g^{-1}$), high mechanical flexibility, ultra-thinness, good electrical conductivity, and high theoretical capacitance (e.g., 550 F g^{-1}), much attentions have been paid to the application of graphene for EESDs [5], in particular, high-energy batteries and high-power supercapacitors (SCs) [6–11]. At present, various methods have been developed to effectively synthesize graphene via top-down or bottom-up strategies. In general, top-down strategies are mainly based on the exfoliation of graphite [12], such as micromechanical cleavage, oxidation-exfoliation-reduction, intercalation exfoliation, and solid exfoliation (e.g., ball milling [13]). And bottom-up strategies include organic synthesis from small structurally-defined molecules (e.g., polyphenylene [14]) and chemical vapor deposition (CVD) [15]. Notably, the graphene products vary distinctly from different synthesis methods in terms of number of layers, sizes, functional groups, wrinkles, defects (in-plane holes or heteroatom doping) and shapes (e.g., graphene nanoribbons), which could be remarkably reflected by huge differences in apparent properties (e.g., SSA, apparent density) and electrochemical performance of EESDs. For instance, mechanically exfoliated graphene sheets (GSs) possess perfect crystallinity without abundant defects. Then they exhibit a low sheet resistance (R_s) of around 400 Ω sq^{-1} at room temperature [16], much higher than that of reduced graphene oxide (rGO) sheets by wet chemical routes, in which many defects and oxygen containing functional groups are left in GSs, therefore, resulting in low conductivities mainly ranging from 298 to 0.045 S m^{-1} are usually obtained [17]. Furthermore, the layers and defects of GSs could be precisely

* Corresponding authors.
E-mail addresses: wuzs@dicp.ac.cn (Z.-S. Wu), wcren@imr.ac.cn (W. Ren).

http://dx.doi.org/10.1016/j.scib.2017.04.010
2095-9273/

prepared by CVD method via adjusting growth parameter (e.g., temperature, time, catalyst), however, in the case of oxidation-exfo liation-reduction, the control of layers and defects seems to be impossible. Therefore, by using appropriately physical or chemical method, one can create desirable defects to adjust the band structure of graphene based materials (e.g., porous graphene and doped graphene sheets), and functionalize graphene with organic/inorganic matters for performance enhancement. Furthermore, GSs could be assembled into macroscopic architectures (e.g., one-dimensional (1D) fibers, two-dimensional (2D) films, three-dimensional (3D) foams) with structural diversity and functional innovations [18], which eventually endow these graphene-enabled EESDs with novel features, such as stretchable lithium ion batteries (LIBs) [19], compression-tolerant SCs [20], on-chip mirco-supercapacitors (Micro-SCs) [21], flexible lithium-sulfur (Li-S) batteries [22], wearable lithium-air (Li-O_2) batteries [23]. Therefore, the synthetic method affects the graphene products and then greatly impacts on their properties for potential electrochemical applications. Specifically, electrochemical exfoliation of graphite may be a good route to produce high conductive GSs as conductive addictive in LIBs, while oxidation-exfoliation-reduction may be suitable for fabricating graphene/metal oxide hybrid for SCs application, in which the intimate interactions between GSs and metal oxide are good for electrochemical performance due to the presence of some oxygen containing functional groups [24].

Despite of widespread efforts, it is still not yet clear whether graphene could be widely used as a major active material or as an inactive additive in electrode of these EESDs [6]. Indeed, there are a large number of scientific publications on graphene-based EESDs with high energy density and power density, most of which outperform the commercial EESDs based on the state-of-the-art materials. However, the results so far reported to date tend to say that the real breakthroughs are still to come. Most importantly, how to bridge the gap between laboratory-based research and practical applications of graphene-based EESDs is fully unsolved.

Here we review the recent progresses of graphene-based materials for different EESDs, e.g., LIBs, SCs, Micro-SCs, Li-O_2 and Li-S batteries (Fig. 1), address the great importance of the pore, doping, assembly, hybridization and functionalization of different nano-architectures in improving their electrochemical performance, and highlight the major roles of graphene of (1) a superior active material, (2) ultrathin 2D flexible support, and (3) an inactive yet electrically conductive additive. Furthermore, we describe the enormous potential of graphene for constructing newly emerging graphene-enabled EESDs with multiple functionalities of light-weight, ultra-flexibility, thinness, and novel cell configurations, and finally, briefly discuss future perspectives and challenges of graphene-based EESDs.

2. Lithium ion batteries

2.1. Graphene electrodes

It is well known that GSs possess a high theoretical lithium storage capacity of 744 mAh g^{-1} if Li ions are attached to both sides of the GSs [25], which is much higher than that of graphite (372 mAh g^{-1}), and the most commonly used anode materials in LIBs. It is noted that both the morphology and microstructure of GSs greatly influence lithium storage. For instance, the GSs with single, triple and quintuplicate layers as anode materials exhibited a high reversible capacity of 1,175, 1,007 and 842 mAh g^{-1}, respectively [26]. Accordingly, decreased size, increased edge sites and increased defects of the GSs are highly benefit for the enhancement of lithium storage [27].

Heteroatom doping could effectively tune the surface chemical properties and electronic band structure, and therefore improve the performance of LIBs. For example, the nitrogen- or boron-doped graphene shows a high reversible capacity of >1,040 mAh g^{-1} at a low rate of 50 mA g^{-1}. More importantly, it can be quickly charged and discharged in a very short time of 1 h to several tens of seconds together with high-rate capability and

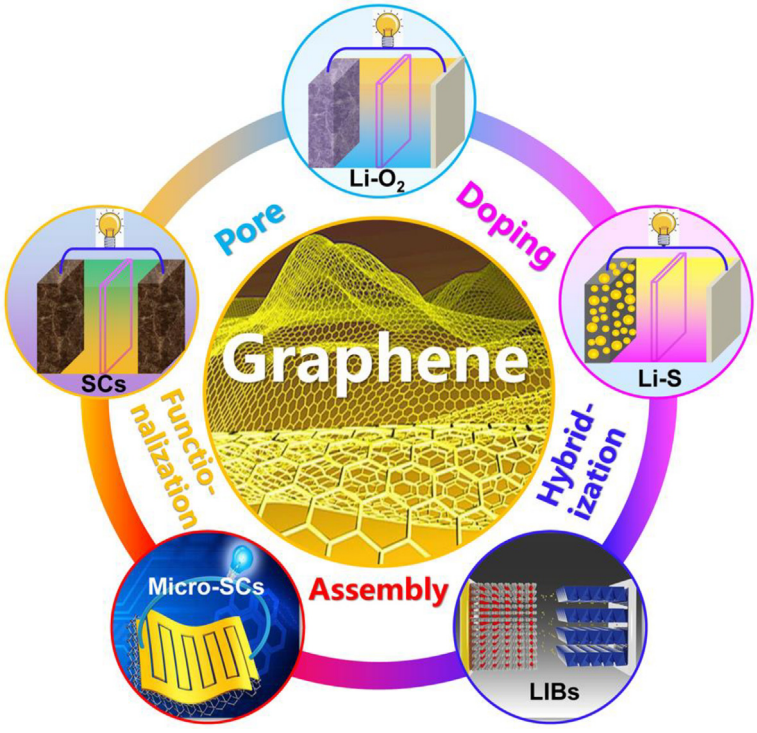

Fig. 1. (Color online) Schematic of graphene-based materials for electrochemical energy storage systems, such as LIBs, Li-S batteries, Li-O_2 batteries, SCs and Micro-SCs.

excellent long-term cyclability. The unique 2D structure, disordered surface morphology, heteroatomic defects, improved electrode/electrolyte wettability, increased inter-sheet distance and electrical conductivity, are beneficial to rapid surface Li^+ absorption and ultrafast Li^+ diffusion and electron transport, and thus make the doped materials superior to those of pristine chemically derived GSs and other carbonaceous materials [28].

Porous graphene has attracted increasing attention because of their rich porosity and high SSA, which would be favorable for fast electrolyte diffusion and electron transport in energy storage [29]. As a typical example, highly ordered mesoporous graphene frameworks with large pore volume ($1.8\ cm^3\ g^{-1}$) and high SSA ($1{,}000\ m^2\ g^{-1}$) exhibit a specific capacity of 520 mAh g^{-1} at a current density of 300 mA g^{-1} after 400 cycles. However, porous GSs with high SSA usually lead to a large irreversible capacity, which greatly prevents its practical application in LIBs.

Graphene nanoribbons (GNRs), a quasi-one-dimensional form of graphene, are favorable for Li^+ storage due to the presence of rich edges [30]. However, pure GNRs only deliver a low capacity of about 250 mAh g^{-1} after 50 cycles [31]. Benefiting from the N doping and edge effect, N-doped GNRs could maintain a stable capacity of 714 mAh g^{-1} after 100 cycles at a current density of 0.1 A g^{-1} and excellent rate capability at high current density of 3 A g^{-1} [32]. Li-ion storage capacity could be further enhanced by creating micrometer-scale interconnected porous structure via assembling N doped GNRs into 3D aerogels. As a result, a high capacity of 910 mAh g^{-1} was achieved at a current density of 0.5 A g^{-1} [33].

The large irreversible capacity related to low Coulombic efficiency in the first cycle as well as capacity fluctuation related to the complex surface chemistry and electrochemical behavior of graphene at the interface of the electrolyte and electrode still represent the major challenging issues for practical use of graphene based materials for LIBs. To address these issues, Wu et al. [34] developed an effective strategy of pre-lithiation surface-modification of graphene with LiF nanoparticles (NPs), which to some extent decreased the first-cycle irreversible capacity, delivered a large specific capacity (>1,500 mAh g^{-1}) at a high rate (>200 mAh g^{-1} at 25 A g^{-1}).

2.2. Graphene/metal oxide electrodes

Transitional metal oxides (e.g., Fe_2O_3, Co_3O_4, SnO_2) have been regarded as promising candidates for large-scale energy storage applications (e.g., electric vehicle and hybrid electric vehicle) because of their higher capacity than that of graphite [35–37]. However, they usually suffer from large volume expansion, poor electrical conductivity and sluggish kinetics for charge transfer and ionic diffusion during the electrochemical reactions [38]. A simple and efficient approach to overcome this obstacle is to synthesize graphene/metal oxide hybrids, which could fully utilize the advantages of both graphene and metal oxides as active materials for energy storage [6,7]. So far, many graphene/metal oxide composites with different structures (Fig. 2) have been developed. It is worth noting that the graphene used in the composite is mainly chemically derived graphene with some oxygen-containing functional groups, such as graphene oxide (GO) and rGO.

Nanostructured metal oxide facilitates high utilization of active materials and accommodation of huge volume expansion during repeatedly charge/discharge cycles, such as mesoporous Fe_3O_4 nanorods [39], SnO_2 nanosheets [40], $NiCo_2O_4$ nanosheets [41], TiO_2 hollow structures [42], have been composited with GSs for high performance LIBs. In our pioneer work, we reported a facile strategy to synthesize the composites of Co_3O_4 NPs (10–30 nm in size) homogeneously anchored on conducting rGO (Fig. 3a). On the one hand, the Co_3O_4 NPs acted as spacers to keep the neighboring GSs separated (Fig. 3b, c). On the other hand, the flexible structure of 2D GSs and strong interaction between Co_3O_4 NPs and GSs in the composite were beneficial for efficiently preventing volume expansion/contraction and aggregation of Co_3O_4 NPs during Li charge/discharge process. Because of this synergistic effect, the Co_3O_4 NPs/graphene composite exhibited a large reversible capacity of 935 mAh g^{-1} after 30 cycles (Fig. 3d), highlighting the combined advantages of anchoring NPs on GSs for the maximum utilization of electrochemically active Co_3O_4 NPs and graphene for high-performance LIBs [43]. The mechanism for the positive synergistic effect was well disclosed in a strong-coupled NiO/rGO hybrid by in situ TEM [44]. Specifically, rGO sheets greatly increased the Li^+ diffusion rate by two orders of magnitude, strongly improved Li^+ reaction kinetics with NiO at high current densities and facilitated homogeneous lithiation of NiO. Furthermore, rGO severely restricted the expansion of NiO (Fig. 3e–g), ensuring stable electrical contact between graphene and NiO in the hybrid during extended cycling process.

To alleviate the huge volume expansion of metal oxide during repeated charge/discharge cycles, porous metal oxides, such as porous iron oxide ribbons [46] and hollow mesoporous $CoFe_2O_4$ nanospheres [47], coupled with graphene, have been fabricated for graphene-based composites. Furthermore, unstable solid electrolyte interphase (SEI) on metal oxide usually deteriorates the integrity of the electrodes, resulting in undesired cycling stability.

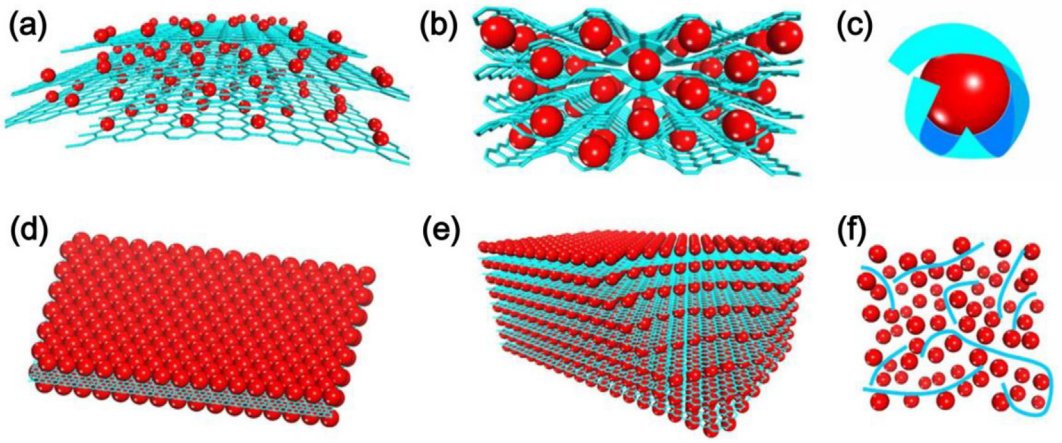

Fig. 2. (Color online) Schematic of structural models of graphene/metal oxide hybrids. (a) Anchored model: oxide NPs anchored on graphene. (b) Wrapped model: oxide wrapped by graphene. (c) Encapsulated model: oxide encapsulated by graphene. (d) Sandwich-like model: an oxide/graphene/oxide sandwich-like structure. (e) Layered model: an alternating layered structure of oxide and graphene. (f) Mixed model: graphene and oxide mechanically mixed. Reprinted with permission from Ref. [7], Copyright © 2012 Elsevier.

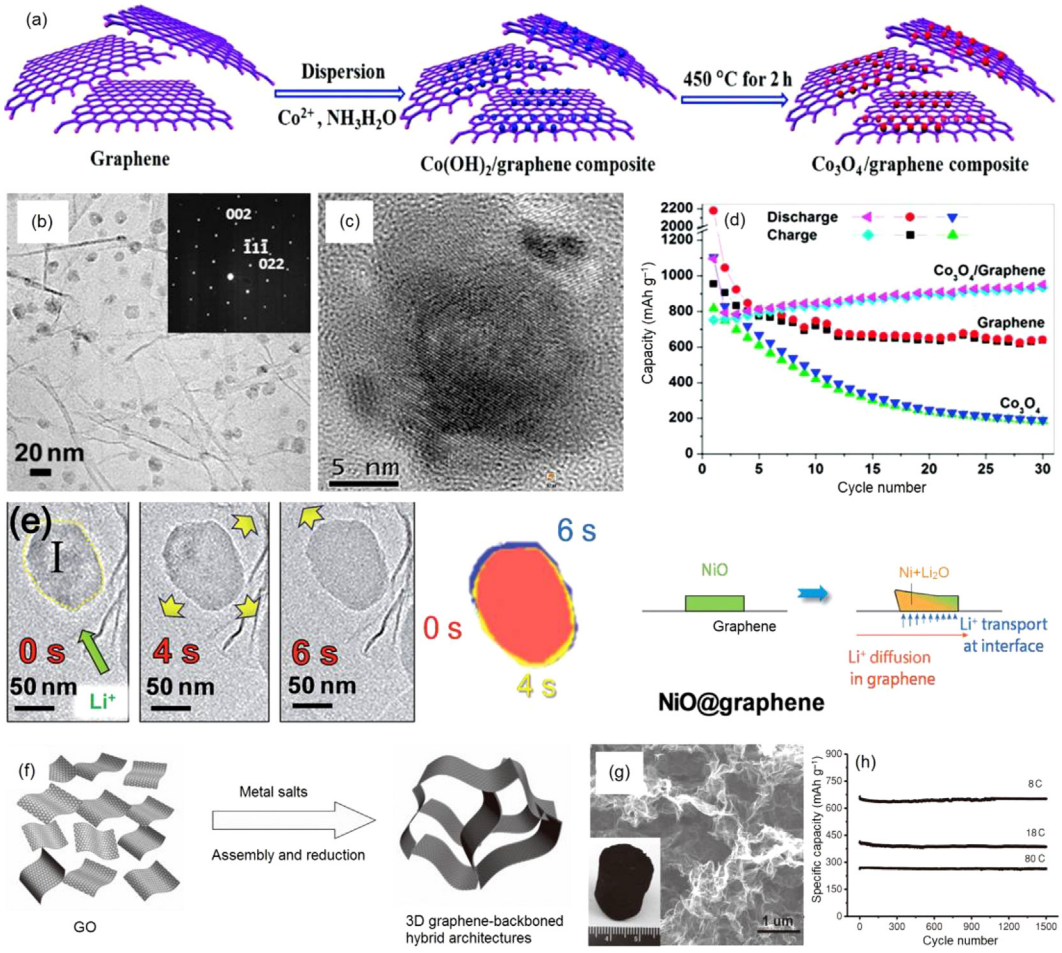

Fig. 3. (Color online) (a) Schematic of the fabrication process of Co_3O_4/graphene composite. (b) Transmission electron microscope (TEM) and (c) high resolution TEM (HRTEM) images of Co_3O_4/graphene composite. (d) Cycling performance of Co_3O_4/graphene composite. Reprinted with permission from Ref. [43], Copyright © 2010 American Chemical Society. (e) Li^+ reaction kinetics with NiO@graphene snapshots for the Li^+ reaction with NiO in NiO@graphene. Reprinted with permission from Ref. [44], Copyright © 2014 The Royal Society of Chemistry. (f) Schematic for fabricating FeO_x-graphene hybrid by a simple hydrothermal method. (g) Scanning electron microscope (SEM) image of FeO_x-graphene hybrid. (h) Cycling stability of FeO_x-graphene at different current densities. Reproduced with permission from [45], Copyright © 2013 John Wiley & Sons, Inc.

Therefore, either conducting polymer or thin carbon layer, which facilitates the formation of a stable SEI layer, is employed to coat metal oxide/graphene hybrids, resulting in 2D sandwich-like sheets, such as carbon-coated graphene/metal oxide (SnO_2 or Fe_3O_4) hybrids [48] or polyaniline coated SnO_2 NPs/GSs [36].

Besides stable cyclic performance, high-rate capability is also important for LIBs, which is closely related to fast electron and ion diffusion in the electrodes. To this end, 3D graphene foams (GFs)/metal oxide hybrids with rich porosity and large SSA have been designed for high-rate electrodes [49]. For instance, 3D FeO_x/-graphene hybrids with SSA of 265 $m^2\ g^{-1}$ and FeO_x content of 85% were synthesized by hydrolysis of $FeCl_3$ in the presence of GO under hydrothermal condition, delivering a capacity of 270 mAh g^{-1} at 80 C even after 1,500 cycles (Fig. 3h) [45]. Similarly, 3D GFs cross-linked with pre-encapsulated Fe_3O_4 nanospheres and graphene aerogels supported with CoO nanostructures were also reported for high-performance LIBs [50,51].

2.3. Flexible graphene based electrodes for LIBs

Recently, thin, lightweight and flexible EESDs have attracted great attentions for next-generation high-performance flexible electronics. GSs with advanced physical and chemical properties could be easily assembled into 2D flexible graphene films and 3D compressible graphene aerogels, bringing new opportunities for flexible graphene based electrodes.

Unfortunately, the closely stacked structure of graphene paper can create barriers for the diffusion of Li ions in electrolyte, preventing individual GSs from the realization of their full potential [52]. However, a free-standing anode could eliminate the use of auxiliary materials (metallic current collectors, conductive carbon black and polymer binder) and consequently increase energy density of the whole cell. The thickness of graphene papers significantly influences the electrochemical performance. For example, Hu et al. [53] found that three types of graphene papers with thickness of 1.5, 3 and 10 μm, fabricated by vacuum-assisted filtration of rGO sheets suspended in water, delivered evidently different lithium storage capacities, and thinner papers always outperformed the thicker ones. Liu et al. [52] prepared a folded structured graphene paper by mechanically pressing graphene aerogel. The folded structure of the GSs with fewer layers can provide more lithium insertion active sites, such as edge-type sites and nanopores.

The face-to-face stacking of rGO sheets in the pore walls is less tight than the stacking of pristine graphene layers in graphite owing to the flexible corrugated structure and colloidal interactions between hydrated rGO sheets containing oxygen functional

groups. Therefore, solvated graphene frameworks (SGFs) through a convenient solvent-exchange approach could achieve a high SSA of approximately 980 $m^2 g^{-1}$ (Fig. S1a, b online), however, a low SSA of 530 $m^2 g^{-1}$ was obtained in the case of freeze dried graphene aerogel (GA) with strong stacking of rGO within the pore walls. Therefore, SGF electrodes could achieve the full potential of 3D graphene and deliver higher capacities at the current densities from 0.2 to 5 A g^{-1} than that of GA electrode (Fig. S1c online) [54].

Incorporating nanostructured active materials with high theoretical specific capacity into GSs could provide more accessible area for better utilization of both the GSs and active materials. These nanostructured active materials include zero-dimensional (0D) SnO_2 or Si NPs [55,56], 1D MnO_2 nanotubes [57], 2D phosphorene sheets [58]. Furthermore, graphene papers could also be acted as substrates for the growth of carbon nanotube (CNT) forest, resulting in free-standing G/CNT anodes in LIBs [59]. Despite of these progresses to date, fast ion transport throughout the 2D sheet-like structure is not well solved yet. Creating in-plane vacancies as new diffusion channels in GSs is a promising approach for high-power LIBs. Zhao et al. [60] first introduced nanometer-sized structural defects into rGO (deGO) by a facile wet chemical method (Fig. S1d online), then prepared a Si-deGO paper hybrid by vacuum-filtration, and the resulting Si-deGO anodes could deliver a high reversible capacity of 1,100 mA g^{-1} at 8 A g^{-1} (Fig. S1e online).

Flexible or compressive GFs with high porosity are ideal conductive substrates for deposition of active materials. Dong et al. [51] used compressive graphene aerogels for the growth of CoO nanostructures, resulting in binder-free graphene aerogel/CoO nanostructured anodes in LIBs, which exhibited superior electrochemical performance to conventional electrodes made of powders and binders. Li et al. [61] designed and synthesized a thin, lightweight, and flexible graphene-based LIB full cell, in which flexible and conductive interconnected GFs grown by CVD were used as current collectors for loading $Li_4Ti_5O_{12}$ (LTO) and $LiFePO_4$ (LFP) as anode and cathode (Fig. S1f online), respectively. The LTO nanosheets stood perpendicular to the surface of the GFs, which not only provided a large interfacial area for fast lithium insertion/extraction but also ensured a short solid-state diffusion length. The LIB full cell could be operated at a high rate of 10 C with a capacity of 117 mAh g^{-1}, and show no structural failure and performance loss even being repeatedly bent to a radius of 5 mm (Fig. S1g, h online).

2.4. Graphene based electrodes for post-LIBs

With the fast development of portable electronics and electrical vehicles, LIBs are facing great challenges due to the high price and uneven distribution of lithium resources. Newly developed batteries, e.g., sodium ion batteries (SIBs), potassium ion batteries (PIBs) and aluminum ion batteries (AIBs), are considered as alternatives of LIBs for large scale electrochemical energy storage. Especially, SIBs are mostly studied post-LIBs due to its rich abundance (Na), low-cost, high theoretical capacities as well as similar redox potentials ($E_{Na+/Na}$=−2.7 V) to lithium ($E_{Li+/Li}$=−3.0 V) [62]. However, larger ionic radius of Na^+ (1.02 Å) in comparison with Li^+ (0.76 Å) results in more sluggish reaction kinetics with lower power/energy density [63]. In this sense, GSs with tunable properties and structural features could be applied in high performance SIBs.

Conductive rGO with large interlayer distances and a disordered structure could exhibit high capacity up to 174.3 mAh g^{-1} at 40 mA g^{-1} as well as long-term cycling life over 1,000 cycles [64]. Heteroatom doping (e.g., N, B, S, and P) of graphene could significantly enhance electrical conductivity and surface hydrophilicity of graphene electrodes to improve the charge transfer and electrode–electrolyte interactions. Furthermore, heteroatom doping could also create additional redox sites for Na^+ storage and induce larger interspacing layers, resulting in superior capacities than that of un-doped GSs. For example, S-doped GSs delivered a large reversible capacity of 291 mAh g^{-1} and high rate capability of 83 mAh g^{-1} at 5.0 A g^{-1} [65]. Free-standing fluorine and nitrogen co-doped graphene paper (FNGP) electrodes showed a reversible capacity of 203 mAh g^{-1} at 50 mA g^{-1} after 100 cycles and long-cycling stability with a capacity of 56.3 mAh g^{-1} after 5,000 cycles at 1 A g^{-1} [66]. 3D interconnected graphene foam showed large surface area for easy electrolyte diffusion and fast electron transfer, greatly facilitating reaction kinetics. 3D N doped graphene foams (N-GF) displayed a high capacity of 594 mAh g^{-1} with 69.7% retention at 500 mA g^{-1} after 150 cycles, outperforming previously reported carbonaceous materials [67].

Similarly to LIBs, graphene-based composites enable SIBs with higher specific capacities, better rate capability and longer cycle life than pure graphene. Various electrochemically active materials with high capacities and poor electrical conductivities, such as metal sulfides/oxides [68–70], phosphorene or red phosphorus [71,72], have been coulped with GSs, in which the presence of GSs could improve the conductivity of them and achieve better nanostructures for Na^+ reaction kinetics and structural stability during repeated charge/discharge cycles.

3. Supercapacitors

Because of high SAA of 2,630 $m^2 g^{-1}$ and extraordinary theoretical capacitance of 550 F g^{-1}, graphene offers tremendous opportunities to ultimately replace the traditional carbon-based materials (such as activated carbon) in SCs [7]. In fact, graphene can act as a superior active material when it participates in the whole charge-storage process, in which electrolyte ions (e.g., Li^+, Na^+) can electrostatically store on the electrode of SCs. However, due to serious agglomeration of GSs caused by strong Van der Waals interaction, graphene surface could be not fully utilized for ion adsorption. The first SCs based on chemically modified GSs only exhibited a low specific capacitance of 135 F g^{-1} in an aqueous electrolyte, which is comparable with the traditional carbon-based electrode materials [73]. Additionally, direct access to the charge-storage surface is severely restricted by the agglomerated structure, leading to a substantial ionic resistance in the electrode.

3.1. High surface area graphene based supercapacitors

To overcome the above mentioned problems, various high SSA graphene based materials have been developed to enhance the ions storage in SCs. Miller et al. [74] synthesized vertically oriented GSs directly on heated Ni substrates using radio frequency plasma-enhanced CVD. The film thickness of vertically oriented GSs was approximately 600 nm, which efficiently prevented the stacking between nanosheets, leading to a high SAA up to 1,100 $m^2 g^{-1}$. Vertically oriented GSs had a preponderance of exposed edge planes that greatly increased charge storage as compared with that relied on basal plane surfaces, open structure greatly reduced ionic resistances, and high conductivity grown from a conductive surface, minimizing electronic resistances. As a result, the SCs made from these GSs exhibited ac line-filtering performance with a RC time constant of <200 μs, which showed a great potential to replace the commercially available electrolytic capacitors.

El-Kady et al. [75] used a standard LightScribe DVD optical drive to conduct direct laser reduction of GO to graphene (Fig. 4a). The produced graphene films were mechanically robust, showed high electrical conductivity (1,738 S m^{-1}) and SSA (1,520 $m^2 g^{-1}$), and could thus be used directly as SC electrodes without need of binders and current collectors, as the case for conventional SCs. There-

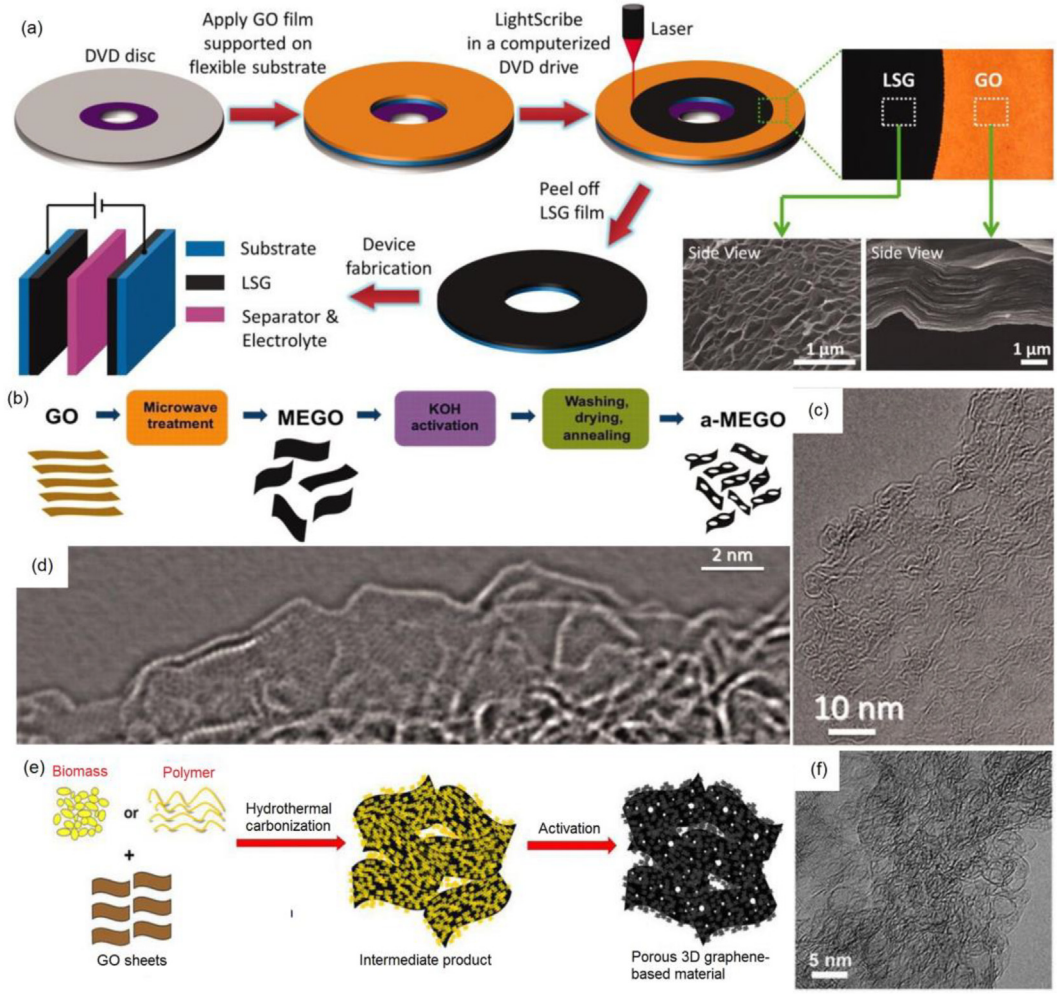

Fig. 4. (Color online) (a) Schematic of the fabrication of LSG-based SCs. Reproduced with permission from Ref. [75], Copyright © 2012 AAAS. (b) Schematic of activated microwave-expanded graphite oxide (a-MEGO). (c) High-resolution phase contrast electron micrograph of the thin edge of a-MEGO. (d) HRTEM image from the edge of a-MEGO. Reproduced with permission from Ref. [76], Copyright © 2011 AAAS. (e) Schematic of the simple and green process of synthesizing porous 3D graphene-based materials. (f) HRTEM image of 3D graphene-based bulk materials showing a 3D porous structure with highly wrinkled surface. Reproduced with permission from Ref. [77], Copyright © 2013 Nature Publishing Group.

fore, the laser-scribed graphene (LSG) SCs exhibited energy density of up to 1.36 mWh cm^{-3}, approximately two times higher than that of a commercial activated-carbon SC. Ruoff's group [76] reported the synthesis of activated graphene with a Brunauer-Emmett-Teller SSA of up to 3,100 $m^2 g^{-1}$ via KOH chemical activation of microwave exfoliated graphite oxide (Fig. 4b). Interestingly, this sp^2-bonded carbon had a continuous 3D network of highly curved (Fig. 4c), atom-thick walls that formed primarily 0.6 to 5-nm-width pores, and substantial curvature of the single-carbon sheets was visible. Meanwhile, the in-plane crystallinity was preserved (Fig. 4d). Two-electrode SC cells constructed with this carbon, yielded high gravimetric capacitance of 166–200 F g^{-1} and superior energy density of ~70 Wh kg^{-1}.

Highly conductive GSs are good 2D building blocks for constructing sandwich-like porous carbon layer/graphene hybrids. Porous 3D graphene-based bulk materials with exceptional high SSA (3,523 $m^2 g^{-1}$) and excellent conductivity (up to 303 S m^{-1}) were fabricated by in-situ hydrothermal polymerization and carbonization of the mixture of cheap biomass or industry carbon sources with GO, followed by a chemical activation process (Fig. 4e) [77]. Due to the defected and wrinkled GSs in the dimensional size of 4–6 nm (Fig. 4f), these materials showed superior supercapacitor performance in ionic liquid with specific capacitance and energy density of 231 F g^{-1} and 98 Wh kg^{-1}, respectively. Yan et al. [78] synthesized interconnected frameworks with a sandwiched porous carbon layer/graphene hybrids by one-step pyrolysis of the mixture of GO/polyaniline and KOH, and the obtained porous carbon material exhibited a high SSA (2,927 $m^2 g^{-1}$), hierarchical interconnected pores, moderate pore volume (1.78 $cm^3 g^{-1}$), and a high nitrogen level (6 at.%). Furthermore, it displayed unprecedented gravimetric capacitance of 481 F g^{-1} in an aqueous electrolyte.

3.2. Graphene based supercapacitors with high volumetric capacitance

Because of the fluffy state of the GSs with high SSA, the packing density of common graphene electrodes is rather low (from 0.05 to 0.75 g cm^{-3}), which would result in low volumetric energy density [79]. By simply compressing a-MEGO as electrode material, a volumetric capacitance of up to 110 F cm^{-3} was achieved in a two-electrode supercapacitor in an organic electrolyte, which was twice of that of uncompressed a-MEGO electrode [80]. It is worth noting that ion diffusion could be not efficiently achieved in most compact graphene materials with limited channels for efficient electrolyte diffusion and transportation, resulting in a low volumetric capacitance. Therefore, rational design of porous structures in

compacted graphene based film electrode is very critical for warranting high volumetric capacitance.

Taking advantage of 2D intrinsic micro-corrugated configuration and self-assembly behavior of rGO, Yang et al. [79] synthesized highly compact carbon electrodes with a continuous ion transport network by capillary compression of adaptive graphene gel films in the presence of a nonvolatile liquid electrolyte (Fig. 5a). The GSs in the films stacked in a nearly face-to-face fashion, and the thicknesses were nearly proportional to the volumetric fraction of incorporated nonvolatile liquids trapped in the gels (Fig. 5b). Most importantly, highly efficient ion transport channels were retained although the packing density was as high as 1.33 g cm^{-3}. Therefore, the resulting liquid electrolyte-mediated rGO film electrode achieved a high volumetric energy density approaching 60 Wh L^{-1}.

GSs with in-plane pores can facilitate ion transfer across the 2D plane of graphene. A holey graphene framework (HGF) was prepared through one-step process with low temperature H_2O_2 etching of nanopores in graphene and self-assembly of graphene into 3D monolithic network (Fig. 5e). A 140-μm HGF electrode with a high packing density of 0.71 g cm^{-3} was synthesized by compressing a piece of 1 cm thick HGF with a packing density of 12 mg cm^{-3} (Fig. 5f, g), which simultaneously delivered a high gravimetric capacitance of 298 F g^{-1} and a volumetric capacitance of 212 F cm^{-3} in organic electrolyte [81].

Hard-template method is an efficient strategy to create desired porous structures. Yan et al. [82] demonstrated the fabrication of functionalized GSs (FGN-300) via low temperature (300 °C) treatment of graphite oxide with a slow heating rate using $Mg(OH)_2$ nanosheets as template (Fig. 5h). Because of its dented sheet with high SSA (285 m^2 g^{-1}), low pore volume (0.47 cm^3 g^{-1}), and a certain amount of oxygen-containing groups (Fig. 5i), the as-obtained graphene delivered ultrahigh volumetric capacitance of 470 F cm^{-3}, 3.3 times higher than hydrazine reduced graphene (Fig. 5j). More importantly, the assembled supercapacitor exhibited an ultrahigh volumetric energy density of 27.2 Wh L^{-1}.

Interestingly, Tao et al. [83] developed a highly dense but porous graphene-based monolithic carbon by evaporation-induced drying of a graphene hydrogel, which integrated a porous microstructure (370 m^2 g^{-1}) and a high density (1.58 g cm^{-3}) (Fig. 5k, l). This conductive graphene material with unimpeded ion transport channels was moldable for a current collector free electrode in a supercapacitor device, resulting in ultrahigh volumetric capacitance up to 376 F cm^{-3} (Fig. 5m). Further, by adding zinc chloride ($ZnCl_2$) during capillary drying of graphene hydrogel, the SSA of the monolithic graphene was tuned from 370 to over 1,000 m^2 g^{-1}, while the monoliths still maintained high density from 1.6 to 0.6 g cm^{-3}. The directly sliced graphene pellet electrode with a thickness up to 400 μm delivered a capacitance of 150 F cm^{-3} in an ionic liquid electrolyte, corresponding to a volumetric energy density of ~65 Wh L^{-1} in a symmetrical SC, which was among the highest values reported to date for SCs [84].

3.3. Flexible graphene based electrodes for supercapacitors

Graphene-based materials possess many excellent properties such as ultrathin flexible 2D structure and superior capacitive performance, which make them ideally suited for use in the flexible

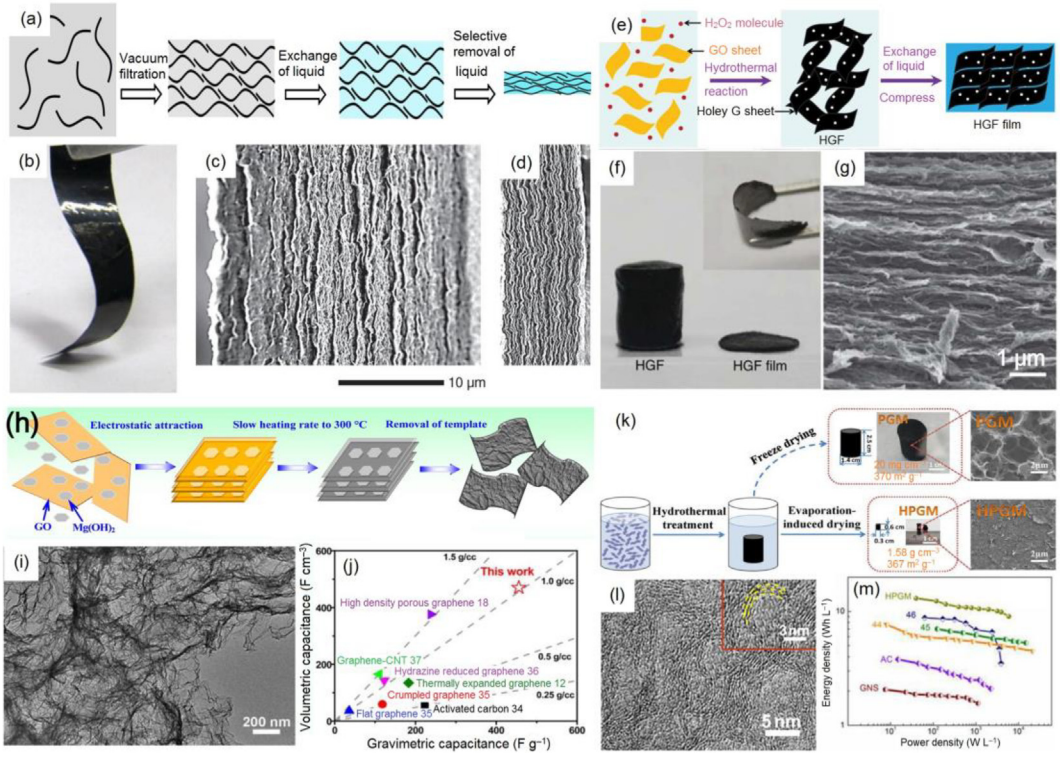

Fig. 5. (a) Schematic showing a soft chemistry route to fabricate electrolyte-mediated rGO film from the rGO dispersion. (b) A photograph showing the flexibility of the film. SEM images of cross sections of the obtained electrolyte-mediated rGO films containing 78.9 vol% (c) and 27.2 vol% (d) of H_2SO_4. Reproduced with permission from Ref. [79], Copyright © 2013 AAAS. (e) Schematic of the preparation process of HGFs and HGF films. (f) A photograph showing HGFs before and after mechanical compression. (g) Cross-sectional SEM image of the compressed HGF film. Reproduced with permission from Ref. [81], Copyright © 2014 Nature Publishing Group. (h) Schematic illustration of the fabrication and (i) TEM image of FGN-300. (j) Comparison of the volumetric and gravimetric capacitances of FGN-300 electrode with other carbon electrodes. Reproduced with permission from Ref. [82], Copyright © 2014 American Chemical Society. (k) Schematic of the formation of graphene-based 3D porous macroforms with different drying processes and SEM images of the resultant PGM and HPGM. (l) TEM image of HPGM. (m) Ragone plot of HPGM in comparison with reported activated carbon (AC), GSs and other carbon materials. Reproduced with permission from Ref. [83], Copyright © 2013 Nature Publishing Group.

and wearable SCs that can endure different mechanical deformations, such as reversible bending, stretching, compressing, and twisting [85]. 3D graphene hydrogels were used for the fabrication of high-performance all-solid-state flexible supercapacitors (Fig. 6a, b) by pressing a graphene hydrogel thin film with a thickness of 120 μm, which could provide a favorable porous structure for electrolyte infiltration to make full use of the large electrical double-layer capacitance of graphene. The fabricated SCs exhibited high gravimetric specific capacitance of 186 F g^{-1} (up to 196 F g^{-1} for a 42 μm thick electrode). Notably, the CV curves obtained at various bending angles showed nearly the same capacitive behavior, demonstrative of extraordinary mechanical flexibility (Fig. 6c) [86].

Highly active transition metal oxides or conducting polymers are generally considered to promote the electrochemical capacitance of GSs. A free-standing flexible graphene/polyaniline composite paper was prepared by in-situ anodic electropolymerization of polyaniline on a graphene paper, and showed a stable electrochemical capacitance (233 F g^{-1} and 135 F cm^{-3} for gravimetric and volumetric capacitances) [88]. Wu et al. [89] developed a large-scale printing technique for the fabrication of ultrathin printable supercapacitors based on graphene-PH1000 conducting polymer, which presented unprecedented performance of ultrahigh scan rate of 2,000 V s^{-1} and AC line-filtering performance. 3D rGO films with high flexibility and interconnected pores created by $CaCO_3$ templates were used as a bendable 3D skeleton for growth of polyaniline (PANI) nanowire arrays, yielding a hierarchical 3D graphene/PANI composite film. Notably, the graphene/PANI film electrode had a specific capacitance of 385 F g^{-1} at 0.5 A g^{-1} as well as high rate capability with capacity retention of 94% at current density of 10 A g^{-1}. Importantly, the film supercapacitor could be bent by 90° and 180° without obvious changes in CV curves (Fig. 6e) [87]. Furthermore, lightweight (0.75 mg cm^{-2}), highly conductive (55 S cm^{-1}) and flexible 3D graphene networks were used as support for loading MnO_2 (mass loading of 9.8 mg cm^{-2}) by electrodeposition. A symmetrical supercapacitor consisting of the sandwich structure of two pieces of 3D graphene/MnO_2 composite network exhibited similar CV behaviors with bending angles of 0° and 90° [90]. MnO_2 and polypyrrole (PPy) were deposited on 3D GF/CNT hybrid film with high flexibility and robustness, resulting GF/CNT/MnO_2 and GF/CNT/PPy hybrids, respectively [91]. The as-fabricated asymmetric GF/CNT/MnO_2//GF/CNT/PPy SCs could deliver high energy density (22.8 Wh kg^{-1} at 860 W kg^{-1}) in 0.5 mol L^{-1} Na_2SO_4 aqueous electrolyte, most importantly, the device could be bent to a large extent without degrading the performance.

Composite films of rGO and polyaniline nanofibers (PANI-NFs) were prepared by vacuum filtration of the mixed dispersions of both components. The composite film had a layered structure, and PANI-NFs were sandwiched between rGO layers. The flexible composite film with high conductivity of 550 S m^{-1} showed large specific capacitance of 210 F g^{-1} at a discharge rate of 0.3 A g^{-1} [92]. Furthermore, a densely packed graphene nanomesh-carbon nanotube film (GNCN) was fabricated through a simple graphene etching process and subsequent vacuum-assisted filtration. The ion diffusion ability of the GNCN film was greatly enhanced due to the contribution of cross-plane diffusion from the graphene nanomesh and in-plane diffusion from the graphene-carbon nanotube sandwiched structure. In addition, carbon nanotubes can also efficiently improve the overall electrical and mechanical properties of the hybrid film. Therefore, the GNCN film electrode exhibited a specific capacitance of 294 F g^{-1} at 5 mV s^{-1}, higher than the rGO film (185 F g^{-1}) [93]. Additionally, 1D NiCo-carbonate hydroxide nanowires or 2D vanadyl phosphate nanosheets were also used to manufacture graphene-based flexible composite films for SCs [94,95].

4. Micro-supercapacitors

Micro-SCs are a newly emerging class of microscale EESDs with advantages of ultrahigh power density, fast charge and discharge rate, and superior cycling stability, which can potentially act as stand-alone power sources for microelectronics [96]. More recently, planar graphene-based Micro-SCs have attracted considerable attention because they can sufficiently utilize the unique structure and properties of graphene, like atomic thinness and high SSA, for efficient energy storage [97–99].

Table S1 (online) presents the state-of-the-art graphene-based Micro-SCs, highlighting the relationship of structure-preparation-performance. For instance, Ajayan's group [21] reported the scalable production of graphene-based monolithic Micro-SCs consisting of rGO micro-electrodes and GO as separator by laser reduction and patterning of GO films, offering an areal capacitance of 0.51 mF/cm^2, nearly twice than that of the stacked SCs. El-Kady and Kaner [98] realized scalable fabrication of graphene Micro-SCs

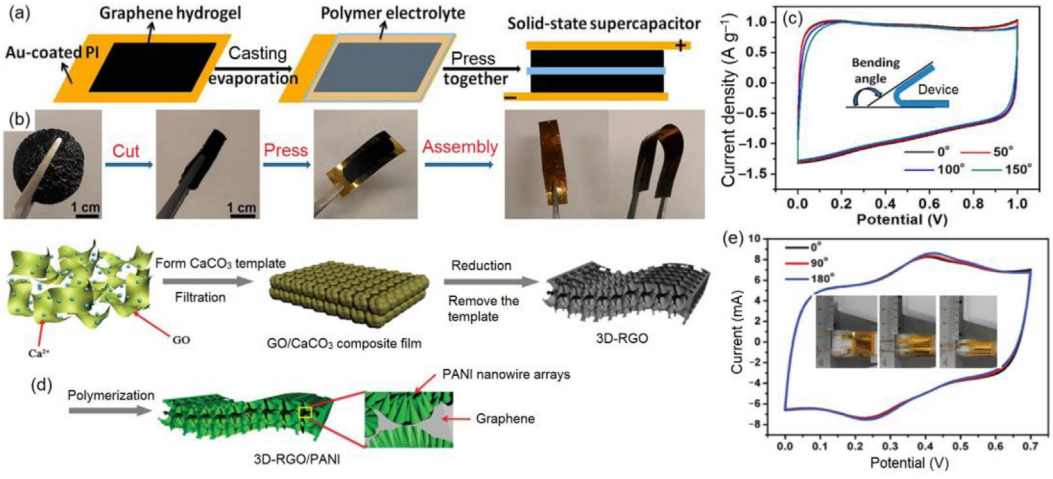

Fig. 6. Schematic (a) and photographs (b) of the fabrication process of flexible all-solid-state supercapacitors based on graphene hydrogel films. (c) CV curves of all-solid-state device for different bending angles. Reproduced with permission from Ref. [86], Copyright © 2013 American Chemical Society. (d) Schematic diagram of the fabrication process of flexible all-solid-state supercapacitors based on 3D graphene/PANI composite films. (e) CV curves of the film supercapacitor bent by 0°, 90° and 180°. Reproduced with permission from Ref. [87], Copyright © 2013 John Wiley & Sons, Inc.

by direct laser writing on graphite oxide films using a standard LightScribe DVD burner (Fig. 7a). More than 100 Micro-SCs could be readily generated on a single disc in 30 min. Micro-SCs with mechanical stability showed exceptional electrochemical stability regardless of the degree of bending or twisting (Fig. 7b, c). Furthermore, four LSG based Micro-SCs could be combined together both in series and in parallel configurations to control the operating voltage and capacity for practical applications (Fig. 7d). Later, Wu et al. [99] developed a novel class of all-solid-state graphene-based in-plane interdigital Micro-SCs on arbitrary substrates through micro-patterning of graphene films with a nanoscale thickness of 6–100 nm. Due to high electrical conductivity (345 S cm^{-1}) of the fabricated graphene films and in-plane geometry of micro-devices for rapid ions transportation along the planar GSs with a short diffusion length, the resulting Micro-SCs could deliver an areal capacitance of 80.7 μF cm^{-2}, a stack capacitance of 17.9 F cm^{-3}, superior power density of 495 W cm^{-3}, and high energy density of 2.5 mWh cm^{-3} that is comparable to lithium thin-film batteries. Subsequently, Wu et al. [100] also reported other high-performance planar Micro-SCs using different graphene materials, e.g., heteroatom-doping graphene films for ultrahigh rate and high volumetric capacitance Micro-SCs (2,000 V s^{-1} and 488 F cm^{-3}).

Recently, our group [101] reported the bottom-up fabrication of continuous, uniform, and ultrathin (~10.0 nm) sulfur-doped graphene (SG) films by thermal annealing of the spray-coated trisulfur-annulated hexa-peri-hexabenzocoronene (SHBC)-based film, with assistance of a thin Au protecting layer. Notably, the as-produced all-solid-state planar SG-MSCs exhibited a highly stable pseudocapacitive behavior with a volumetric capacitance of ~582 F cm^{-3} at 10 mV s^{-1} and ultrahigh power density of ~1,191 W cm^{-3}. Our group [102] also demonstrated a versatile printable technology to fabricate arbitrary shaped, printable graphene-based planar sandwich supercapacitors based on the layer-structured film of electrochemically exfoliated graphene (EG) as two electrodes and nanosized GO (lateral size of 100 nm) as a separator on one substrate, which exhibited outstanding volumetric capacitance of ~280 F cm^{-3}.

Pseudocapacitive active materials with high theoretical specific capacitance are often combined with GSs to improve the electrochemical performance of Micro-SCs. Recently, Wu et al. [103] developed a general method for the fabrication of alternating

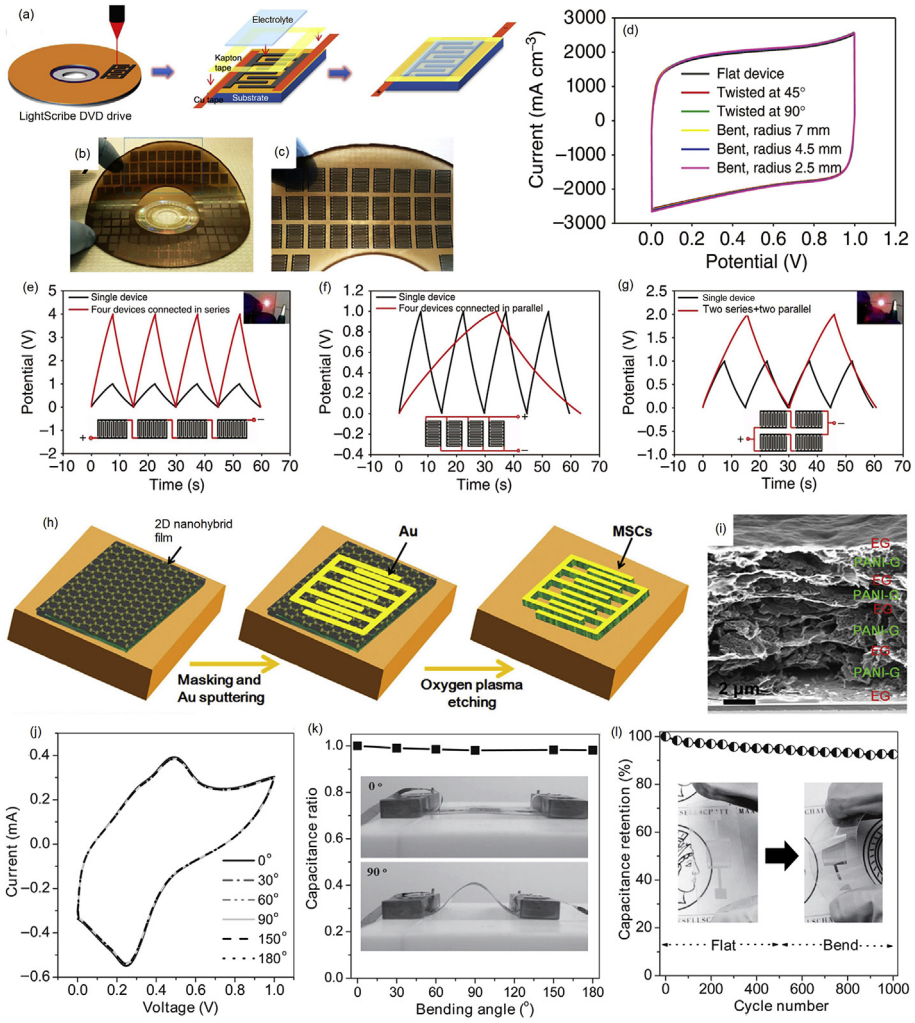

Fig. 7. (a) Schematic of the fabrication process for LSG-based Micro-SCs. (b, c) Photographs of LSG-based Micro-SCs bent with a tweezers and 112 micro-devices on a DVD disk. (d) CVs of LSG-based Micro-SCs tested at different bending states. Galvanostatic charge/discharge curves for four tandem Micro-SCs connected (e) in series, (f) in parallel and (g) in a combination of series and parallel. Reproduced with permission from Ref. [98], Copyright © 2013 Nature Publishing Group. (h) Schematic of fabrication procedure for graphene-conducting polymer based Micro-SCs. (i) Cross-section SEM image of graphene-conducting polymer film for Micro-SCs. (j) CVs of graphene-conducting polymer based Micro-SCs tested at different bending states. (k) Evolution of the capacitance ratio as a function of bending angle. (l) Cycling stability of graphene-conducting polymer based Micro-SCs under flat and bending state. Reproduced with permission from Ref. [100], Copyright © 2014 John Wiley & Sons, Inc.

stacked graphene-polymer films for compact in-plane Micro-SCs based on a layer-by-layer stacked 2D hybrid film of electrochemically EG and graphene-based mesoporous polyaniline (PANI-G) sheets (Fig. 7h). The hybrid film showed a densely layer-stacked feature, remarkable conductivity, and high mass density of 1.67 g cm^{-3} (Fig. 7i). Importantly, the unique alternating stacked structure with a strong coupling effect from the 2D pseudocapacitive PANI-G and capacitive EG sheets endowed the graphene-polymer film for Micro-SCs with good cycling stability under different bending angles (Fig. 7j, k) or constant bending state (Fig. 7l) [103]. Liu et al. [104] reported a printing technique for the fabrication of Micro-SCs by spray-coating the EG/PH1000 hybrid ink through a customized mask with the designed interdigital geometry. The fabricated Micro-SCs on a paper substrate offered a significant areal capacitance as high as 5.4 mF cm^{-2}. Furthermore, our group [105] developed stacked-layer thiophene (TP)/EG heterostructure films (TP/EG) with a thickness of ~105 nm produced by alternating deposition of EG nanosheets (≤3 layers) and redox-active conducting TP nanosheets (thickness of 3.5 nm) in sequence. The resulting TP/EG-MSCs could offer a landmark areal capacitance of 1.30 mF cm^{-2} and volumetric capacitance of 123 F cm^{-3} at 100 V s^{-1}. Pseudo-capacitive MnO_2 possesses high redox capacitance (theoretically 1,300 F g^{-1}). Peng et al. [106] first prepared δ-MnO_2/graphene hybrids by chemically integrating δ-MnO_2 nanosheets on graphene, and then fabricated δ-MnO_2/graphene based planar SCs. Due to more electrochemically active surfaces for absorption/desorption of electrolyte ions, and additional interfaces at the hybridized interlayer areas to facilitate charge transport during charging/discharging processes, the δ-MnO_2/graphene based Micro-SCs exhibited excellent electrochemical performance, such as high specific capacitance of 267 F g^{-1} at current density of 0.2 A g^{-1}, and 208 F g^{-1} at 10 A g^{-1}, and excellent cycling stability with capacitance retention of 92% after 7,000 cycles.

5. Lithium air batteries

Lithium-air (oxygen) batteries offer much higher energy density than LIBs. For example, the theoretical energy density of lithium-oxygen batteries can reach 5,200 Wh kg^{-1}. The recharge ability of this system basically relies on the conversion of reduction products of Li_2O_2 and LiO_2 during oxygen reduction reaction (ORR), and return to the initial products during oxygen evolution reaction (OER). However, the ORR/OER processes are sluggish with high over-potentials and low energy efficiencies, which further cause significant electrolyte decomposition and hence a short battery lifespan [107]. The requirements of an O_2 electrode combine high SSA, high electrical conductivity and strong electrocatalytic activity to the ORR and OER [108]. In this case, 2D graphene is considered as a promising cathode material for Li-O_2 batteries. Indeed, graphene could deliver higher capacities of 11,060 mAh g^{-1} at 280 mA g^{-1} than commercial carbon (~5,100 mAh g^{-1}) [109]. However, the relatively inert nature of graphene leads to poor wettability and weak contacts with electrolytes and Li_2O_2 as well as less catalytic assistance in ORR and OER during discharging and charging. As a consequence, short cycling life and poor rate capability are usually not avoided.

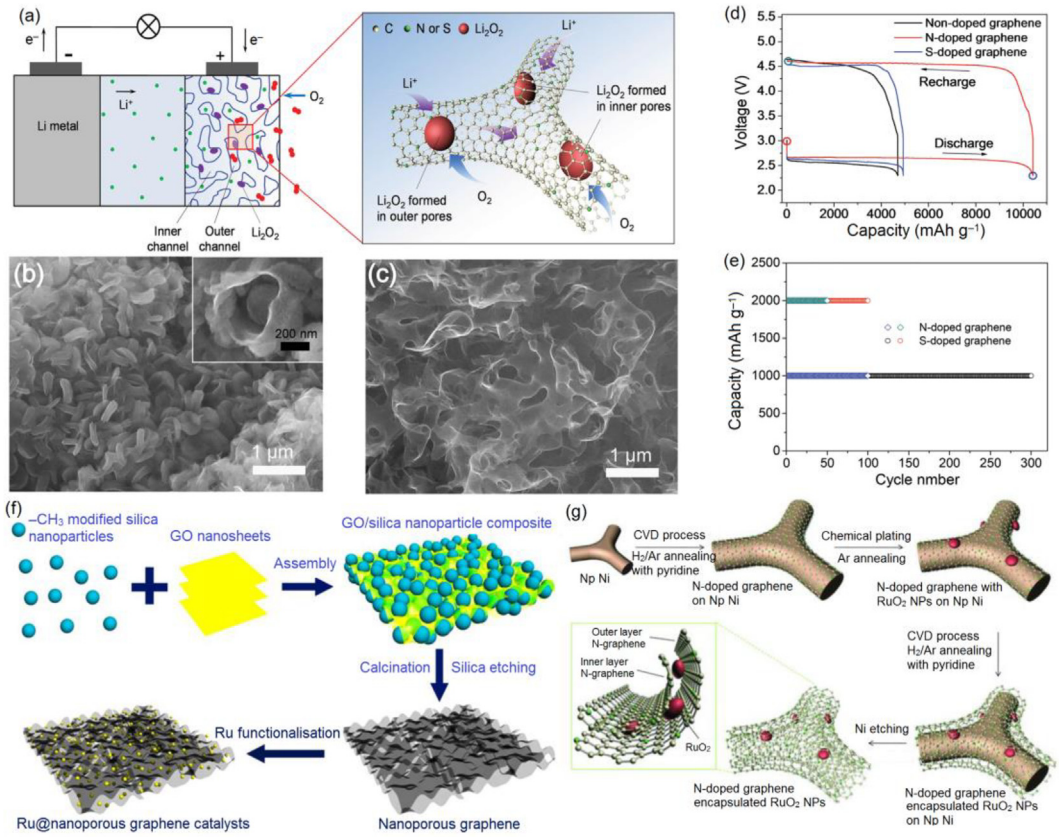

Fig. 8. (a) Schematic of a nanoporous graphene based Li-O_2 battery. Cross-sectional SEM images of fully discharged (b) and fully recharged (c) N-doped graphene electrodes. (d) Galvanostatic discharge-charge profiles of Li-O_2 cells using non-, N- and S-doped graphene cathodes. (e) Cycling stability of nanoporous N- and S-doped graphene based Li-O_2 cells. Reproduced with permission from Ref. [110], Copyright © 2016 John Wiley & Sons, Inc. (f) Schematic for synthesis of porous graphene and Ru-functionalized nanoporous graphene architectures. Reproduced with permission from Ref. [111], Copyright © 2014 American Chemical Society. (g) Schematic of the preparation of nanoporous N-doped graphene with encapsulated RuO_2 NPs. Reproduced with permission from Ref. [112], Copyright © 2015 John Wiley & Sons, Inc.

Chemical doping of graphene could effectively tailor the charge density and surface chemical properties, resulting in enhanced electrochemical performance of Li-O_2 batteries. For example, chemical doping and 3D bicontinuous porous configuration can dramatically improve the electrode reaction kinetics of graphene (Fig. 8). This material was synthesized by CVD on nanoporous metal with benzene, pyridine, or thiophene as carbon, nitrogen, or sulfur sources, respectively. The high reversibility of Li_2O_2 formation and decomposition in the ultra-large capacity was further confirmed by SEM images of the discharged and recharged N-doped graphene electrodes (Fig. 8b, c). The non-, N-, and S-doped graphene samples have SSA of 1,220, 772 and 775 $m^2\ g^{-1}$, respectively, which are three to four times higher than other commonly-reported graphene materials. The porous structure with the average pore size of 230–260 nm would provide many channels for efficient oxygen and electrolyte diffusion and sufficient spaces for Li_2O_2 deposition without electrode damage as well as expose more electrochemically active sites. Chemical doping contributed to the enhanced ORR reaction kinetics that was further confirmed by the gradual decrease in the over potentials for discharging from non-doped, S-doped to N-doped graphene (Fig. 8d). The maximum discharge capacities from non-doped, S-doped and N-doped graphene were measured to be 4,690, 4,920 and 10,400 mAh g^{-1}, respectively. Impressively, N-doped and S-doped graphene based Li-O_2 batteries reached 100 and 300 cycles at the cut-off capacity of 1,000 mAh g^{-1} (Fig. 8e). 3D porous N-doped graphene nanocages with interconnected channels and fully exposed active sites could be modulated by polystyrene sphere@polydopamine. The resulting graphene-based electrode exhibited an excellent capacity of 5,978 mAh g^{-1} at 3.2 A g^{-1}, and long cycle stability at a large current density (54 cycles at 1 A g^{-1}) [113]. Except N or S doped graphene, boron atoms have been doped into the carbon lattices of graphene to greatly activate the electrons in the carbon π system for fast charge under large current densities. Density functional theory calculation demonstrated that B doped graphene exhibited very strong interactions with Li_5O_6 clusters, therefore, B-doped graphene effectively activated Li−O bonds to decompose Li_2O_2 during charge [114]. In addition, N and S co-doped graphene with tunable doping contents could exhibit excellent electrochemical performance [115].

Another efficient approach to enhance the cathodic reaction kinetics for low charge over potentials and high energy efficiency is to integrate high active catalysts with graphene nanomaterials. By far, various noble metals or metal oxides, such as Ru [111], Au [116], RuO_2 [112], MnO_2 [117], Co_3O_4 [118] and $MnCo_2O_4$ [119], have been employed to decorate with graphene in Li-O_2 batteries. For example, Ru nanocrystal-decorated porous graphene exhibited a charge voltage plateau at 3.15 V, which was much lower than that of the porous graphene electrode without Ru decoration (4.3 V) (Fig. 8f) [111]. In most cases, the weak bonding between NPs and graphene by physical adsorption usually leads to the coarsening and agglomeration of catalyst NPs and hence quick degeneration and short lifetimes of Li-O_2 batteries. To avoid these shortcomings, one efficient approach is to construct noble metals or metal oxides/graphene hybrids with strongly coupled interfaces. For example, covalently coupled $MnCo_2O_4$/graphene hybrids were synthesized by direct nucleation and growth of $MnCo_2O_4$ NPs on the surface of rGO. Interestingly, $MnCo_2O_4$/graphene cathode possessed similar low charge-discharge over-potential to that of Pt/C cathode, but displayed a longer cycle life [119]. Another efficient approach is to embed catalysts into graphene materials. For instance, Guo et al. [112] developed a novel 3D nanoporous cathode by encapsulating RuO_2 NPs with nanoporous N-doped graphene (Fig. 8g), and the RuO_2 NPs were still encapsulated by 2–3 layers of N-doped graphene after discharge/charge cycles, while nanoporous N-doped graphene with un-encapsulated RuO_2 NPs became coarsening after about 62 cycles.

6. Lithium-sulfur batteries

Li-S battery is a high-energy electrochemical system with a theoretical energy density of 2,600 Wh kg^{-1}, based on the redox reaction between elemental sulfur and Li (S_8 + 16Li ↔ 8Li_2S) [120,121]. However, three problems greatly hinder the commercialization of Li-S batteries: (1) low electrical and Li^+-ionic conductivity of elemental sulfur and solid sulfides (Li_2S_2 and Li_2S), which increases the internal resistance of the battery and impedes the full utilization of the active materials. (2) Non-negligible volume expansion up to 80% from sulfur to Li_2S, which severely reduces the mechanical integrity of the electrode. (3) The soluble nature of the polysulfides (Li_2S_x, $4 < x < 8$) in organic electrolytes, which leads to the mass loss of sulfur and notorious shuttle effect. In this regard, graphene has been widely used for sulfur based cathodes, interlayers, separators, current collectors and even Li anodes in Li-S batteries to overcome these issues (Table S2 online).

6.1. Graphene based materials for sulfur cathodes

GSs have been used to physically or chemically alleviate shuttle effects in S based cathodes. Uniformly dispersed sulfur on rGO sheets (63.6wt% S content) can deliver a reversible capacity of 804 mAh g^{-1} after 80 cycles at 312 mA g^{-1} and 440 mAh g^{-1} after 500 cycles at 1,250 mA g^{-1} [122].

Considering that non-polar GSs are incompatible with polar discharge products (Li_2S_2/Li_2S). The detachment and separation of Li_2S from GSs usually result in fast capacity fade. Therefore, functionalized graphene materials with polar sites, such as N-doped graphene [123], hydroxylated graphene [124], amino-functionalized rGO [124], have been developed to greatly immobilize sulfur and to avoid sulfur loss during repeated charge/discharge cycles for prolonged life. For example, nitrogen-containing groups on graphene could efficiently bind polar lithium polysulfides (Fig. 9a), therefore, N-doped GSs (NG) enabled the cell to achieve ultra-long cycle life exceeding 2000 cycles, and extremely low capacity-decay rate (0.028%/cycle) [123]. In addition, 2D flexible GSs have been employed as coating layers to accommodate volume expansion of sulfur particles during discharge, trap soluble polysulfide intermediates, and render sulfur particles electrically conducting [125,128]. For example, rGO sheets were coated on a thermally exfoliated graphene sheet-sulfur (TG-S) composite to physically restrain the diffusion of polysulfides (Fig. 9b) [125].

Microporous/mesoporous structures could act as nano-reactors to improve the conductivity of sulfur, accommodate the volume expansion and effectively suppress the diffusion of polysulfide species [126,127,129]. KOH-activated rGO sheets with high SSA (2,313 $m^2\ g^{-1}$) and pore volume (1.8 $cm^3\ g^{-1}$) endowed high specific capacity up to 1,379 mAh g^{-1} at 0.2 C and excellent cycling stability [130]. Sandwich-type micro/mesoporous carbon layer/graphene sheets (SCNMM) were well designed by a double template method, using GO as the shape-directing agent and SiO_2 NPs as the mesoporous guide (Fig. 9c). Such a design of hybrid carbon sheets as a sulfur immobilizer led to good cycle stability (860 mAh g^{-1} at 1 C after 100 cycles) and good rate capability (510 mAh g^{-1} at 10 C) [126]. CVD is a controllable and effective method to synthesize novel graphene materials with unique nanostructures due to the large-scale selections of various templates or catalysts. MgAl-layered double oxide (LDO) flakes obtained by the calcination of MgAl layered double hydroxides (LDHs) were adopted as mesoporous catalysts for the templated growth of unstacked double-layer template graphene (DTG) com-

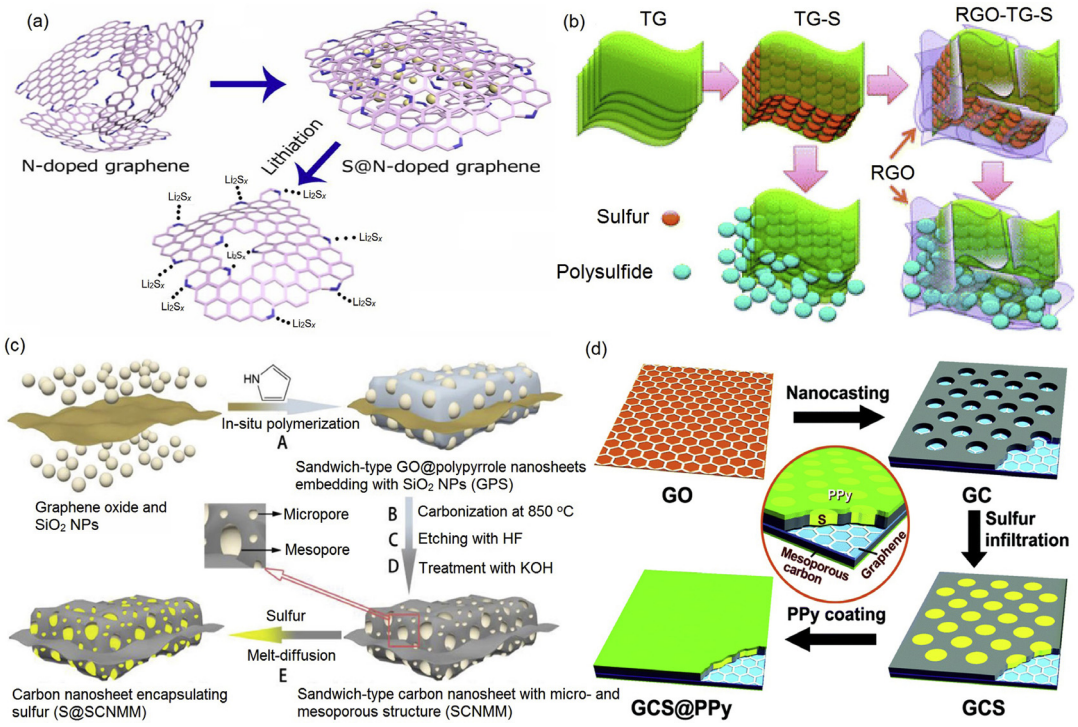

Fig. 9. (a) Schematic of the synthesis of S@NG composite and N functional groups for trapping Li_2S_x. Reproduced with permission from Ref. [123], Copyright © 2014 American Chemical Society. (b) Scheme of RGO-TG-S composite for improving cathode performance. Reproduced with permission from Ref. [125], Copyright © 2012 Royal Society of Chemistry. (c) Scheme of the procedure for preparing S@SCNMM. Reproduced with permission from Ref. [126], Copyright © 2014 John Wiley & Sons, Inc. (d) Schematic of synthesizing GCS@PPy hybrid sheets. Reproduced with permission from Ref. [127], Copyright © 2015 Royal Society of Chemistry.

posed of two graphene layers with a large quantity of protuberances, and the DTG with only a few layers (<3) of graphene possessed a thickness of ca.10 nm and a high SSA of 1,628 $m^2 g^{-1}$. As a result, the DTG/S hybrid delivered high reversible capacities of 530 and 380 mAh g^{-1} even after 1000 cycles at 5 and 10 C, respectively [131]. $Mg_2Zn_{0.1}Al$ LDH was also adopted for the rational combination of Kirkendall diffusion and reduction-induced metal evaporation toward hierarchical oxide templates for CVD self-assembly of 3D porous graphene frameworks (PGFs) with a high SSA of 1,448 $m^2 g^{-1}$ and a mesopore volume of 2.40 $cm^3 g^{-1}$, and the PGFs could achieve a high sulfur utilization of 71% and a low capacity fading rate of ~0.04% per cycle after the second cycle at 1.0 C [132]. Furthermore, porous CaO was employed as both the catalyst and template for CVD growth of hierarchical porous graphene [133]. However, in most cases, the physical barrier provided by open nanopores can only slow down the escape of polysulfides for a short time, therefore, a PPy thin layer was coated on the top surface of nanosized sulfur infiltrated graphene-based mesoporous carbon (denoted as GCS@PPy) (Fig. 9d). In this case, nanostructured S was fully encapsulated by conductive substrates, as a result, high reversible capacity for as long as 400 cycles with ultra-slow decay rate of 0.05% per cycle was achieved at the high rate of 1–3 C [127].

GSs are also favorable for constructing flexible graphene based S cathodes with high energy densities, in which polymer binders and Al current collectors are not required. Recently, freestanding paper-like rGO-S composite films with outstanding flexibility were fabricated by synchronously reducing and assembling GO sheets with S NPs on a Zn foil (Fig. S2a online). The rGO-S films possessed porous structure with interconnected walls, while the S NPs were homogeneously attached on the surface of rGO sheets (Fig. S2b). Two kinds of flexible rGO-S composite based Li-S battery devices in soft-packaged and cable-typed configurations were designed. More importantly, benefiting from effective pathways for electron transport and suppression of the polysulfides diffusion, both devices showed stable electrochemical performance under bending (Fig. S2f–i online) [22]. Dual-confined flexible sulfur cathodes were constructed mainly by graphene wrapping of sulfur/N-doped carbon hollow spheres, in which sulfur/polysulfides were effectively immobilized through physical confinement by the hollow spheres and graphene wrapping as well as chemical binding between hetero nitrogen atoms and polysulfides [134]. Quasi-one-dimensional graphene nanoribbons were also employed for flexible graphene based cathodes. For example, Liu et al. [135] synthesized free-standing sulfur/reduced GO nanoribbon papers (RGONRs) (30.8 μm thick) through S^{2-} reduction and evaporation-induced self-assembly processes (Fig. S2j, k online). The self-weaved graphene nanoribbons were homogeneously coated with sulfur (Fig. S2i–n online), which could bear repeated charge/discharge cycles without any mechanical cracks (Fig. S2o, p online). Therefore, a discharge capacity of 455 mAh g^{-1} was still maintained even after 300 cycles.

6.2. Graphene based interlayers

Because of the relative big pores in commercial polypropylene (PP) separators, physical blocking of polysulfide diffusion to Li anode is negligible. Functional graphene based interlayers existing between S based cathode and separator could rationally regulate the channel sizes for ion transfer and design surface characteristics, thus physically and chemically preventing soluble polysulfides penetrating through separator [136,137]. For instance, Zhou et al. [138] designed an integrated electrode by continuously coating graphene onto one side of a typical commercial PP separator (G@PP separator), in which 30-μm-thick graphene membrane acted as an internal current collector to support 40-μm-thick sulfur layer (Fig. 10a). X-ray microtomography (XRM) images of the integrated electrode before and after cycling confirmed sulfur particle refinement and redistribution in the active material layer and

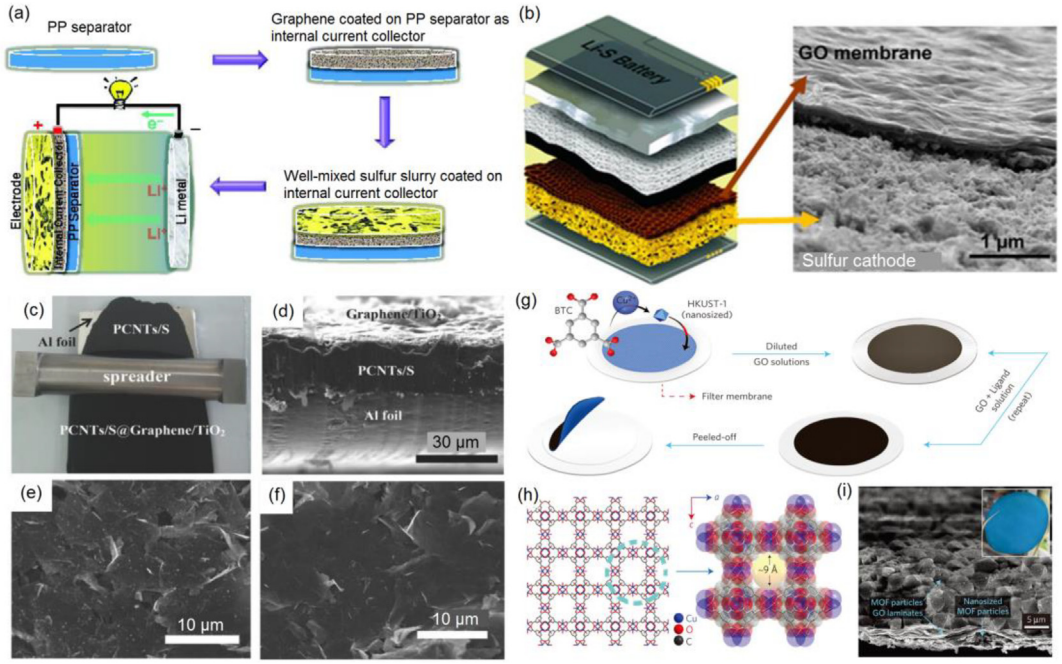

Fig. 10. (Color online) (a) Schematic of the electrode configuration using an integrated structure of sulfur and G@PP separator and the corresponding battery assembly. Reproduced with permission from Ref. [138], Copyright © 2015 John Wiley & Sons, Inc. (b) Schematic of a Li-S cell with a GO-coated sulfur cathode facing a carbon-coated separator. Reproduced with permission from Ref. [139], Copyright © 2016 American Chemical Society. (c) Photograph of graphene/TiO_2 film coating process. (d) Cross-sectional SEM image of fresh cathode with graphene/TiO_2 film. Typical front-view SEM images of graphene/TiO_2 film (e) and neat graphene coating film (f). Reproduced with permission from Ref. [140], Copyright 2015 John Wiley & Sons, Inc. (g) Schematic of the fabrication process to produce MOF@GO separators. (h) Illustration of the microporous crystalline structure (HKUST-1). (i) SEM image of multilayered MOF@GO separator, and the inset shows a digital photo along the MOF side. Reproduced with permission from Ref. [141], Copyright © 2016 Nature Publishing Group.

graphene membrane. Due to the close contact and strong adhesion between sulfur and graphene membrane, the S-G@PP separator cell exhibited specific capacity of 512 mAh g^{-1} at an ultrahigh current density of 12 A g^{-1}, superior to that of the G-S+PP separator cell (139 mAh g^{-1}) and the Al foil-S+PP separator electrode. A high-flux GO membrane was also fabricated directly onto a sulfur cathode by shear alignment of discotic nematic liquid crystals of GO (Fig. 10b). Together with a carbon-coated separator, highly ordered structure of the thin membrane (0.75 μm) and the inherent surface charge effectively retained a majority of the polysulfides, delivering high capacities of about 835 mAh g^{-1} after 100 cycles [139].

Introducing polar sites on non-polar GSs would be benefited for immobilizing polar polysulfides by chemisorption. For this purpose, Wang et al. [142] employed a lightweight S-N dual-doped graphene (SNGE) as a multifunctional porous interlayer, and found that SNGE had outstanding conductivity, high ability to trap polysulfides and modulate Li_2S_2/Li_2S growth, and the functionality to protect separator integrity. Therefore, the SNGE interlayer enabled the porous-CNT/S cathode to deliver impressive electrochemical performance, such as high rate capacity of 130 mAh g^{-1} at 40 C (1 C = 1,675 mAh g^{-1}) and ultrahigh cyclability at 8 C for 1,000 cycles. Furthermore, boron-functionalized rGO layer coated on the separator, PP-supported cellular graphene framework based Janus separator and ternary-layered PP/GO/Nafion separator were also designed to suppress the shuttle effect [143–145]. Polar metal oxide NPs were decorated with graphene based interlayer. Xiao et al. [140] applied lightweight graphene/TiO_2 film as an interlayer on the surface of the porous carbon nanotubes (PCNTs)-S cathode (Fig. 10c–f), which accounted for only 7.8wt% of the whole cathode. The graphene/TiO_2 interlayer could mitigate the polysulfides diffusion and enable the Li-S battery to deliver a reversible specific capacity of 1,040 mAh g^{-1} over 300 cycles at 0.5 C.

Metal-organic framework (MOF)-based materials have a large SSA and highly ordered pores with tunable porosity, which can act as ionic sieves to mitigate the polysulfide ions. As a representative example, Bai et al. [146] designed a ordered microporous (0.9 nm) $Cu_3(BTC)_2$ (HKUST-1) MOF@GO separator without PP utilization, in which the GO laminates not only strengthened the permeation barrier, but also provided a strong support for improving the stability as a separator (Fig. 10g–i). As a result, the battery with the MOF@GO separator possessed low capacity-fading rates of approximately 0.019% per cycle over 1,500 cycles [141]. Subsequently, a Zn(II)-based MOF@GO separator was also employed to minimize the soluble polysulfide migrating to the anode.

6.3. Graphene based current collectors

In contrast to heavy and nonporous Al foil current collector with smooth surface for limited sulfur loading, graphene based current collectors usually provide rough surface or porous channels for more sulfur loading, and thus show promising applications in high-energy Li-S batteries [147,148]. Typically, Zhou et al. [147] reported a graphene membrane based current collector (GCC) for sulfur loading. The average roughness (0.98 μm) of the GCC was approximately three times bigger than that of an Al-foil current collector (0.34 μm) (Fig. S3a, b online). Furthermore, the density of GCC was only 1.3 mg cm^{-2}, one quarter of that of an Al-foil current collector, therefore, the GCC could further significantly improve specific energy density of GCC based Li-S batteries. Most importantly, the porous and layered structured GCC with more accessible SSA would effectively absorb soluble polysulfides during charge and discharge cycles (Fig. S3c, d online).

Specific emphasis is given to the advance of 3D CVD-grown GFs as current collectors for high-energy Li-S batteries [15,148,149]. Compared with the commonly used planar current collectors, GFs

exhibited sufficiently robust and flexible by poly(dimethyl siloxane) (PDMS) coating (Fig. S3e online), which offered efficient space for a high sulfur loading up to 10.1 mg cm^{-2} (Fig. S3f online). Furthermore, the interconnected GFs provided efficient electron pathways and held sufficient electrolyte. As a result, a high areal capacity of 13.4 mAh cm^{-2} (at 300 mA g^{-1}) was achieved (Fig. S3g online), demonstrating the advantages of 3D porous GFs for high energy Li-S batteries [149]. However, GFs have very large pores with limited SSA and are lack of functional groups for anchoring sulfur. To solve these problems, Hu et al. [148] developed a 3D graphene foam-reduced GO (GF-rGO) hybrid nested hierarchical network macrostructure (Fig. S3h, i online). As current collector in Li-S battery, this material could realize high sulfur loading of 14.36 mg cm^{-2} and sulfur content of 89.4wt% simultaneously. Meanwhile, it served as electrolyte reservoir and effectively accommodated the volume expansion of sulfur during charge/discharge cycles. Additionally, highly conductive and porous network could facilitate fast ion and electron transport, and the residual oxygen functional groups on rGO provided anchoring sites to trap the soluble polysulfide intermediates within the electrode. Very impressively, the GF-rGO/S cathodes with a sulfur loading of 9.8 mg cm^{-2} and sulfur content of 83wt% showed a high areal capacity of 10.3 mAh cm^{-2} at 0.2 C with good cycling stability (Fig. S3j online).

7. Conclusions and perspectives

Graphene based materials with distinct characteristics are playing more and more important roles in EESDs, such as ultra-high SSA graphene for large ion storage in electric double layer capacitors, functionalized graphene for anchoring other active species in both SCs and LIBs, highly flexible and conductive graphene based membranes as either interlayers or current collectors in Li-S batteries, heteroatom doped graphene with macroporous structure for catalytic growth/decomposition and accommodation of Li_2O_2 in Li-O_2 batteries. Overall, the presence of graphene in these EESDs have substantially improved their energy/power density and cycling life, superior to that of common materials (e.g., commercial activated carbon, fullerene, carbon nanotubes) and other 2D non-conductive materials.

Despite enormous advances, several challenging issues still remain unsolved: (1) The most important challenge lies in the controllable preparation of graphene-based materials with desired defects (e.g., nanopores, heteroatom doping), SSA and surface chemistry at low cost and high yield for various specific applications. (2) Graphene products synthesized by different methods vary distinctly in term of number of layers, surface properties, lateral sizes, defects and conductivity. Therefore, the desired graphene products must be selected from various graphene products. For example, as the additives in LIBs, high conductive GSs synthesized by intercalation and exfoliation method could be the best choice, while as separators in LIBs, non-conductive GO sheets with oxygen containing functional groups may be the right one. Thereby different-type graphene products should be reasonably chosen in terms of the corresponding EESDs. (3) As a versatile building block, graphene could construct various nanostructures with specific functionalities, so a major issue to be considered is how to simultaneously achieve high volumetric and gravimetric capacity of these EESDs by structural design of graphene based materials. And one possible solution may be to employ different graphene products or nanostructures in one EESD, in which each graphene material or nanostructure may deal with one specific issue. Therefore, various challenges in one EESD are expected to be synergistically solved [150]. (4) rGO sheets with abundant defects and exposed surface area would induce the formation of irreversible lithium ion storage in LIBs and the decomposition of electrolytes in Li-O_2 batteries. So how to effectively tune the surface chemical properties of graphene to avoid the above problems without obvious performance degradation is still a pressing needing.

During the past years, graphene based materials have exhibited improved electrochemical performance in EESDs in terms of cycling life and energy/power density, showing new opportunities for developing high performance electrodes. Notwithstanding the aforementioned progress to date, the practical application of graphene in EESDs still remains its infancy. As a typical example, the market supply of conductive agent in LIBs is still carbon black instead of GSs. On the one hand, most of GS products on the market contain a small amount of metal impurity, and could not meet the high quality requirements for LIBs. On the other hand, new technological innovations are expected to come, such as new electrolyte systems with less sensibility of impurities in GSs, in that case, the available GSs products could be directly applied in LIBs industry. Furthermore, Li metal anodes were extensively studied in the past years for future high-energy-density lithium batteries (e.g., Li-S batteries, Li-O_2 batteries) due to high theoretical capacity (3,860 mAh g^{-1}) and low electrochemical potential [151]. Although graphene products could also serve as collector for dendrite free Li metal deposition and stable solid electrolyte interphase [152,153], there are so many scientific confusions as well as technological challenges for application in Li metal anodes, and the question that what kind of graphene products could be applied in Li metal anodes is still not well answered.

Moreover, the information society is asking for devices with unique features or shapes for some specific applications. As mentioned above, GSs could be easily assembled into 1D fiber, 2D film and 3D bulk materials without the disappearance of the superior properties of GSs, perfectly meeting the requirements of lightweight, flexible, compressible electrodes with designable shapes for wearable and portable devices. Moreover, new-concept EESDs are also highly required for smart devices, such as electrochromic SCs [154], self-healing LIBs [155], smart SCs [156], even integration of EESDs and solar/mechanical energy harvesting devices [157]. Undoubtedly, graphene with intriguing properties could play more important roles in EESDs, promising the coming era of graphene based EESDs in the near future.

Conflict of interest

The authors declare that they have no conflict of interest.

Acknowledgments

This work was supported by the National Key Research and Development Program of China (2016YBF0100100, 2016YFA0200101, and 2016YFA0200200), the National Natural Science Foundation of China (51572259, 51325205, 51290273, and 51521091), the Natural Science Foundation of Liaoning Province (201602737), the Thousand Youth Talents Plan of China (Y5610121T3), China Postdoctoral Science Foundation (2016M601349) and dedicated funds for methanol conversion from Dalian Institute of Chemical Physics, Chinese Academy of Sciences.

Appendix A. Supplementary data

Supplementary data associated with this article can be found, in the online version, at http://dx.doi.org/10.1016/j.scib.2017.04.010.

References

[1] Choi NS, Chen Z, Freunberger SA, et al. Challenges facing lithium batteries and electrical double-layer capacitors. Angew Chem Int Ed 2012;51:9994–10024.
[2] Xiong J, Han C, Li Z, et al. Effects of nanostructure on clean energy: big solutions gained from small features. Sci Bull 2015;60:2083–90.
[3] Geim AK, Novoselov KS. The rise of graphene. Nat Mater 2007;6:183–91.
[4] Allen MJ, Tung VC, Kaner RB. Honeycomb carbon: a review of graphene. Chem Rev 2010;110:132–45.
[5] Yu M, Li R, Wu M, et al. Graphene materials for lithium-sulfur batteries. Energy Storage Mater 2015;1:51–73.
[6] Raccichini R, Varzi A, Passerini S, et al. The role of graphene for electrochemical energy storage. Nat Mater 2015;14:271–9.
[7] Wu ZS, Zhou G, Yin LC, et al. Graphene/metal oxide composite electrode materials for energy storage. Nano Energy 2012;1:107–31.
[8] Sun Y, Wu Q, Shi G. Graphene based new energy materials. Energy Environ Sci 2011;4:1113–32.
[9] Lv W, Li Z, Deng Y, et al. Graphene-based materials for electrochemical energy storage devices: opportunities and challenges. Energy Storage Mater 2016;2:107–38.
[10] Wu H, Zhang Y, Cheng L, et al. Graphene based architectures for electrochemical capacitors. Energy Storage Mater 2016;5:8–32.
[11] Zheng S, Wu ZS, Wang S, et al. Graphene-based materials for high-voltage and high-energy asymmetric supercapacitors. Energy Storage Mater 2017;6:70–97.
[12] Ren W, Cheng HM. The global growth of graphene. Nat Nanotechnol 2014;9:726–30.
[13] Jeon IY, Shin YR, Sohn GJ, et al. Edge-carboxylated graphene nanosheets via ball milling. Proc Natl Acad Sci USA 2012;109:5588–93.
[14] Dössel L, Gherghel L, Feng X, et al. Graphene nanoribbons by chemists: nanometer-sized, soluble, and defect-free. Angew Chem Int Ed 2011;50:2540–3.
[15] Chen Z, Ren W, Gao L, et al. Three-dimensional flexible and conductive interconnected graphene networks grown by chemical vapour deposition. Nat Mater 2011;10:424–8.
[16] Novoselov KS, Geim AK, Morozov SV, et al. Electric field effect in atomically thin carbon films. Science 2004;306:666.
[17] Pei S, Cheng HM. The reduction of graphene oxide. Carbon 2012;50:3210–28.
[18] Cong HP, Chen JF, Yu SH. Graphene-based macroscopic assemblies and architectures: An emerging material system. Chem Soc Rev 2014;43:7295–325.
[19] Sun Y, Lopez J, Lee HW, et al. A stretchable graphitic carbon/Si anode enabled by conformal coating of a self-healing elastic polymer. Adv Mater 2016;28:2455–61.
[20] Zhao Y, Liu J, Hu Y, et al. Highly compression-tolerant supercapacitor based on polypyrrole-mediated graphene foam electrodes. Adv Mater 2013;25:591–5.
[21] Gao W, Singh N, Song L, et al. Direct laser writing of micro-supercapacitors on hydrated graphite oxide films. Nat Nanotechnol 2011;6:496–500.
[22] Cao J, Chen C, Zhao Q, et al. A flexible nanostructured paper of a reduced graphene oxide–sulfur composite for high-performance lithium-sulfur batteries with unconventional configurations. Adv Mater 2016;28:9629–36.
[23] Liu QC, Liu T, Liu DP, et al. A flexible and wearable lithium-oxygen battery with record energy density achieved by the interlaced architecture inspired by bamboo slips. Adv Mater 2016;28:8413–8.
[24] Wu ZS, Wang DW, Ren W, et al. Anchoring hydrous RuO_2 on graphene sheets for high-performance electrochemical capacitors. Adv Funct Mater 2010;20:3595–602.
[25] Hsieh CT, Lin JY, Mo CY. Improved storage capacity and rate capability of Fe_3O_4–graphene anodes for lithium-ion batteries. Electrochim Acta 2011;58:119–24.
[26] Tong X, Wang H, Wang G, et al. Controllable synthesis of graphene sheets with different numbers of layers and effect of the number of graphene layers on the specific capacity of anode material in lithium-ion batteries. J Solid State Chem 2011;184:982–9.
[27] Li X, Hu Y, Liu J, et al. Structurally tailored graphene nanosheets as lithium ion battery anodes: an insight to yield exceptionally high lithium storage performance. Nanoscale 2013;5:12607–15.
[28] Wu ZS, Ren W, Xu L, et al. Doped graphene sheets as anode materials with superhigh rate and large capacity for lithium ion batteries. ACS Nano 2011;5:5463–71.
[29] Wang DW, Li F, Liu M, et al. 3D aperiodic hierarchical porous graphitic carbon material for high-rate electrochemical capacitive energy storage. Angew Chem Int Ed 2008;120:379–82.
[30] Uthaisar C, Barone V, Peralta JE. Lithium adsorption on zigzag graphene nanoribbons. J Appl Phys 2009;106:113715.
[31] Lin J, Peng Z, Xiang C, et al. Graphene nanoribbon and nanostructured SnO_2 composite anodes for lithium ion batteries. ACS Nano 2013;7:6001–6.
[32] Liu Y, Wang X, Dong Y, et al. Nitrogen-doped graphene nanoribbons for high-performance lithium ion batteries. J Mater Chem A 2014;2:16832–5.
[33] Liu Y, Wang X, Wan W, et al. Multifunctional nitrogen-doped graphene nanoribbon aerogels for superior lithium storage and cell culture. Nanoscale 2016;8:2159–67.
[34] Wu ZS, Xue LL, Ren WC, et al. A LiF nanoparticle-modified graphene electrode for high-power and high-energy lithium ion batteries. Adv Funct Mater 2012;22:3290–7.
[35] Nitta N, Wu F, Lee JT, et al. Li-ion battery materials: present and future. Mater Today 2015;18:252–64.
[36] Dong Y, Zhao Z, Wang Z, et al. Dually fixed SnO_2 nanoparticles on graphene nanosheets by polyaniline coating for superior lithium storage. ACS Appl Mater Interfaces 2015;7:2444–51.
[37] Song L, Yang S, Wei W, et al. Hierarchical SnO_2 nanoflowers assembled by atomic thickness nanosheets as anode material for lithium ion battery. Sci Bull 2015;60:892–5.
[38] Wang Z, Zhou L, Lou XW. Metal oxide hollow nanostructures for lithium-ion batteries. Adv Mater 2012;24:1903–11.
[39] Zhou Q, Zhao Z, Wang Z, et al. Low temperature plasma synthesis of mesoporous Fe_3O_4 nanorods grafted on reduced graphene oxide for high performance lithium storage. Nanoscale 2014;6:2286–91.
[40] Ding S, Luan D, Boey FYC, et al. SnO_2 nanosheets grown on graphene sheets with enhanced lithium storage properties. Chem Commun 2011;47:7155–7.
[41] Gao G, Wu HB, Lou XW. Citrate-assisted growth of $NiCo_2O_4$ nanosheets on reduced graphene oxide for highly reversible lithium storage. Adv Energy Mater 2014;4:1400422.
[42] Chen JS, Wang Z, Dong XC, et al. Graphene-wrapped TiO_2 hollow structures with enhanced lithium storage capabilities. Nanoscale 2011;3:2158–61.
[43] Wu ZS, Ren WC, Wen L, et al. Graphene anchored with Co_3O_4 nanoparticles as anode of lithium ion batteries with enhanced reversible capacity and cyclic performance. ACS Nano 2010;4:3187–94.
[44] Shan XY, Zhou G, Yin LC, et al. Visualizing the roles of graphene for excellent lithium storage. J Mater Chem A 2014;2:17808–14.
[45] Gong Y, Yang S, Liu Z, et al. Graphene-network-backboned architectures for high-performance lithium storage. Adv Mater 2013;25:3979–84.
[46] Yang S, Sun Y, Chen L, et al. Porous iron oxide ribbons grown on graphene for high-performance lithium storage. Sci Rep 2012;2:427.
[47] Dong Y, Chui YS, Yang X, et al. Facile synthesis of hollow mesoporous $CoFe_2O_4$ nanospheres and graphene composites as high-performance anode materials for lithium-ion batteries. ChemElectroChem 2015;2:1010–8.
[48] Su Y, Li S, Wu D, et al. Two-dimensional carbon-coated graphene/metal oxide hybrids for enhanced lithium storage. ACS Nano 2012;6:8349–56.
[49] Qiu HJ, Liu L, Wang Y. Template-directed fabrication of 3D graphene-based composite and their electrochemical energy-related applications. Sci Bull 2016;61:443–50.
[50] Wei W, Yang S, Zhou H, et al. 3D graphene foams cross-linked with pre-encapsulated Fe_3O_4 nanospheres for enhanced lithium storage. Adv Mater 2013;25:2909–14.
[51] Dong Y, Liu S, Wang Z, et al. Compressible graphene aerogel supported CoO nanostructures as a binder-free electrode for high-performance lithium-ion batteries. RSC Adv 2015;5:8929–32.
[52] Liu F, Song S, Xue D, et al. Folded structured graphene paper for high performance electrode materials. Adv Mater 2012;24:1089–94.
[53] Hu Y, Li X, Geng D, et al. Influence of paper thickness on the electrochemical performances of graphene papers as an anode for lithium ion batteries. Electrochim Acta 2013;91:227–33.
[54] Xu Y, Lin Z, Zhong X, et al. Solvated graphene frameworks as high-performance anodes for lithium-ion batteries. Angew Chem Int Ed 2015;127:5435–40.
[55] Wang X, Cao X, Bourgeois L, et al. N-doped graphene-SnO_2 sandwich paper for high-performance lithium-ion batteries. Adv Funct Mater 2012;22:2682–90.
[56] Wang JZ, Zhong C, Chou SL, et al. Flexible free-standing graphene-silicon composite film for lithium-ion batteries. Electrochem Commun 2010;12:1467–70.
[57] Yu A, Park HW, Davies A, et al. Free-standing layer-by-layer hybrid thin film of graphene-MnO_2 nanotube as anode for lithium ion batteries. J Phys Chem Lett 2011;2:1855–60.
[58] Chen L, Zhou G, Liu Z, et al. Scalable clean exfoliation of high-quality few-layer black phosphorus for a flexible lithium ion battery. Adv Mater 2016;28:510–7.
[59] Li S, Luo Y, Lv W, et al. Vertically aligned carbon nanotubes grown on graphene paper as electrodes in lithium-ion batteries and dye-sensitized solar cells. Adv Energy Mater 2011;1:486–90.
[60] Zhao X, Hayner CM, Kung MC, et al. In-plane vacancy-enabled high-power Si–graphene composite electrode for lithium-ion batteries. Adv Energy Mater 2011;1:1079–84.
[61] Li N, Chen Z, Ren W, et al. Flexible graphene-based lithium ion batteries with ultrafast charge and discharge rates. Proc Natl Acad Sci USA 2012;109:17360–5.
[62] Yabuuchi N, Kubota K, Dahbi M, et al. Research development on sodium-ion batteries. Chem Rev 2014;114:11636–82.
[63] Mei Y, Huang Y, Hu X. Nanostructured ti-based anode materials for Na-ion batteries. J Mater Chem A 2016;4:12001–13.
[64] Wang YX, Chou SL, Liu HK, et al. Reduced graphene oxide with superior cycling stability and rate capability for sodium storage. Carbon 2013;57:202–8.
[65] Wang X, Li G, Hassan FM, et al. Sulfur covalently bonded graphene with large capacity and high rate for high-performance sodium-ion batteries anodes. Nano Energy 2015;15:746–54.
[66] An H, Li Y, Gao Y, et al. Free-standing fluorine and nitrogen co-doped graphene paper as a high-performance electrode for flexible sodium-ion batteries. Carbon 2017;116:338–46.

[67] Xu J, Wang M, Wickramaratne NP, et al. High-performance sodium ion batteries based on a 3D anode from nitrogen-doped graphene foams. Adv Mater 2015;27:2042–8.
[68] Choi SH, Ko YN, Lee JK, et al. 3D MoS_2-graphene microspheres consisting of multiple nanospheres with superior sodium ion storage properties. Adv Funct Mater 2015;25:1780–8.
[69] Qu B, Ma C, Ji G, et al. Layered SnS_2-reduced graphene oxide composite–A high-capacity, high-rate, and long-cycle life sodium-ion battery anode material. Adv Mater 2014;26:3854–9.
[70] Chen C, Wen Y, Hu X, et al. Na^+ intercalation pseudocapacitance in graphene-coupled titanium oxide enabling ultra-fast sodium storage and long-term cycling. Nat Commun 2015;6:6929.
[71] Sun J, Lee HW, Pasta M, et al. A phosphorene-graphene hybrid material as a high-capacity anode for sodium-ion batteries. Nat Nanotechnol 2015;10:980–5.
[72] Song J, Yu Z, Gordin ML, et al. Chemically bonded phosphorus/graphene hybrid as a high performance anode for sodium-ion batteries. Nano Lett 2014;14:6329–35.
[73] Stoller MD, Park S, Zhu Y, et al. Graphene-based ultracapacitors. Nano Lett 2008;8:3498–502.
[74] Miller JR, Outlaw RA, Holloway BC. Graphene double-layer capacitor with ac line-filtering performance. Science 2010;329:1637–9.
[75] El-Kady MF, Strong V, Dubin S, et al. Laser scribing of high-performance and flexible graphene-based electrochemical capacitors. Science 2012;335:1326–30.
[76] Zhu YW, Murali S, Stoller MD, et al. Carbon-based supercapacitors produced by activation of graphene. Science 2011;332:1537–41.
[77] Zhang L, Zhang F, Yang X, et al. Porous 3D graphene-based bulk materials with exceptional high surface area and excellent conductivity for supercapacitors. Sci Rep 2013;3:1408.
[78] Yan J, Wang Q, Lin C, et al. Interconnected frameworks with a sandwiched porous carbon layer/graphene hybrids for supercapacitors with high gravimetric and volumetric performances. Adv Energy Mater 2014;4:1400500.
[79] Yang X, Cheng C, Wang Y, et al. Liquid-mediated dense integration of graphene materials for compact capacitive energy storage. Science 2013;341:534–7.
[80] Murali S, Quarles N, Zhang LL, et al. Volumetric capacitance of compressed activated microwave-expanded graphite oxide (a-MEGO) electrodes. Nano Energy 2013;2:764–8.
[81] Xu Y, Lin Z, Zhong X, et al. Holey graphene frameworks for highly efficient capacitive energy storage. Nat Commun 2014;5:4554.
[82] Yan J, Wang Q, Wei T, et al. Template-assisted low temperature synthesis of functionalized graphene for ultrahigh volumetric performance supercapacitors. ACS Nano 2014;8:4720–9.
[83] Tao Y, Xie X, Lv W, et al. Towards ultrahigh volumetric capacitance: graphene derived highly dense but porous carbons for supercapacitors. Sci Rep 2013;3:2975.
[84] Li H, Tao Y, Zheng X, et al. Ultra-thick graphene bulk supercapacitor electrodes for compact energy storage. Energy Environ Sci 2016;9:3135–42.
[85] Wen L, Li F, Cheng HM. Carbon nanotubes and graphene for flexible electrochemical energy storage: from materials to devices. Adv Mater 2016;28:4306–37.
[86] X Xu Y, Lin Z, Huang X, et al. Flexible solid-state supercapacitors based on three-dimensional graphene hydrogel films. ACS Nano 2013;7:4042–9.
[87] Meng Y, Wang K, Zhang Y, et al. Hierarchical porous graphene/polyaniline composite film with superior rate performance for flexible supercapacitors. Adv Mater 2013;25:6985–90.
[88] Wang DW, Li F, Zhao J, et al. Fabrication of graphene/polyaniline composite paper via in situ anodic electropolymerization for high-performance flexible electrode. ACS Nano 2009;3:1745–52.
[89] Wu ZS, Liu Z, Parvez K, et al. Ultrathin printable graphene supercapacitors with ac line-filtering performance. Adv Mater 2015;27:3669–75.
[90] He Y, Chen W, Li X, et al. Freestanding three-dimensional graphene/MnO_2 composite networks as ultralight and flexible supercapacitor electrodes. ACS Nano 2013;7:174–82.
[91] Liu J, Zhang L, Wu HB, et al. High-performance flexible asymmetric supercapacitors based on a new graphene foam/carbon nanotube hybrid film. Energy Environ Sci 2014;7:3709–19.
[92] Wu Q, Xu Y, Yao Z, et al. Supercapacitors based on flexible graphene/polyaniline nanofiber composite films. ACS Nano 2010;4:1963–70.
[93] Jiang L, Sheng L, Long C, et al. Densely packed graphene nanomesh-carbon nanotube hybrid film for ultra-high volumetric performance supercapacitors. Nano Energy 2015;11:471–80.
[94] Wu C, Lu X, Peng L, et al. Two-dimensional vanadyl phosphate ultrathin nanosheets for high energy density and flexible pseudocapacitors. Nat Commun 2013;4:2431.
[95] Wan W, Li L, Zhao Z, et al. Ultrafast fabrication of covalently cross-linked multifunctional graphene oxide monoliths. Adv Funct Mater 2014;24:4915–21.
[96] Wu ZS, Feng X, Cheng HM. Recent advances in graphene-based planar micro-supercapacitors for on-chip energy storage. Natl Sci Rev 2014;1:277–92.
[97] Yoo JJ, Balakrishnan K, Huang J, et al. Ultrathin planar graphene supercapacitors. Nano Lett 2011;11:1423–7.
[98] El-Kady MF, Kaner RB. Scalable fabrication of high-power graphene micro-supercapacitors for flexible and on-chip energy storage. Nat Commun 2013;4:1475.
[99] Wu ZS, Parvez K, Feng X, et al. Graphene-based in-plane micro-supercapacitors with high power and energy densities. Nat Commun 2013;4:2487.
[100] Wu ZS, Parvez K, Winter A, et al. Layer-by-layer assembled heteroatom-doped graphene films with ultrahigh volumetric capacitance and rate capability for micro-supercapacitors. Adv Mater 2014;26:4552–8.
[101] Wu ZS, Tan YZ, Zheng S, et al. Bottom-up fabrication of sulfur-doped graphene films derived from sulfur-annulated nanographene for ultrahigh volumetric capacitance micro-supercapacitors. J Am Chem Soc 2017;139:4506–12.
[102] Zheng S, Tang X, Wu ZS, et al. Arbitrary-shaped graphene-based planar sandwich supercapacitors on one substrate with enhanced flexibility and integration. ACS Nano 2017;11:2171–9.
[103] Wu ZS, Parvez K, Li S, et al. Alternating stacked graphene-conducting polymer compact films with ultrahigh areal and volumetric capacitances for high-energy micro-supercapacitors. Adv Mater 2015;27:4054–61.
[104] Liu Z, Wu ZS, Yang S, et al. Ultraflexible in-plane micro-supercapacitors by direct printing of solution-processable electrochemically exfoliated graphene. Adv Mater 2016;28:2217–22.
[105] Wu ZS, Zheng Y, Zheng S, et al. Stacked-layer heterostructure films of 2D thiophene nanosheets and graphene for high-rate all-solid-state pseudocapacitors with enhanced volumetric capacitance. Adv Mater 2017;29:1602960.
[106] Peng L, Peng X, Liu B, et al. Ultrathin two-dimensional MnO_2/graphene hybrid nanostructures for high-performance, flexible planar supercapacitors. Nano Lett 2013;13:2151–7.
[107] Shui J, Lin Y, Connell JW, et al. Nitrogen-doped holey graphene for high-performance rechargeable Li-O_2 batteries. ACS Energy Lett 2016;1:260–5.
[108] Shui JL, Karan NK, Balasubramanian M, et al. Fe/N/C composite in Li-O_2 battery: studies of catalytic structure and activity toward oxygen evolution reaction. J Am Chem Soc 2012;134:16654–61.
[109] Wang ZL, Xu D, Xu JJ, et al. Graphene oxide gel-derived, free-standing, hierarchically porous carbon for high-capacity and high-rate rechargeable Li-O_2 batteries. Adv Funct Mater 2012;22:3699–705.
[110] Han J, Guo X, Ito Y, et al. Effect of chemical doping on cathodic performance of bicontinuous nanoporous graphene for Li-O_2 batteries. Adv Energy Mater 2016;6:1501870.
[111] Sun B, Huang X, Chen S, et al. Porous graphene nanoarchitectures: an efficient catalyst for low charge-overpotential, long life, and high capacity lithium-oxygen batteries. Nano Lett 2014;14:3145–52.
[112] Guo X, Liu P, Han J, et al. 3D nanoporous nitrogen-doped graphene with encapsulated RuO_2 nanoparticles for Li-O_2 batteries. Adv Mater 2015;27:6137–43.
[113] Zhao C, Yu C, Liu S, et al. 3d porous N-doped graphene frameworks made of interconnected nanocages for ultrahigh-rate and long-life Li-O_2 batteries. Adv Funct Mater 2015;25:6913–20.
[114] Wu F, Xing Y, Li L, et al. Facile synthesis of boron-doped rGO as cathode material for high energy Li-O_2 batteries. ACS Appl Mater Interfaces 2016;8:23635–45.
[115] Huang H, Zhu J, Zhang W, et al. Controllable codoping of nitrogen and sulfur in graphene for highly efficient Li-oxygen batteries and direct methanol fuel cells. Chem Mater 2016;28:1737–45.
[116] Wang G, Tu F, Xie J, et al. High-performance Li-O_2 batteries with controlled Li_2O_2 growth in graphene/Au-nanoparticles/Au-nanosheets sandwich. Adv Sci 2016;3:1500339.
[117] Cao Y, Wei Z, He J, et al. α-MnO_2 nanorods grown in situ on graphene as catalysts for Li-O_2 batteries with excellent electrochemical performance. Energy Environ Sci 2012;5:9765–8.
[118] Zhang J, Li P, Wang Z, et al. Three-dimensional graphene-Co_3O_4 cathodes for rechargeable Li-O_2 batteries. J Mater Chem A 2015;3:1504–10.
[119] Wang H, Yang Y, Liang Y, et al. Rechargeable Li-O_2 batteries with a covalently coupled $MnCo_2O_4$-graphene hybrid as an oxygen cathode catalyst. Energy Environ Sci 2012;5:7931–5.
[120] Wang Z, Dong Y, Li H, et al. Enhancing lithium-sulphur battery performance by strongly binding the discharge products on amino-functionalized reduced graphene oxide. Nat Commun 2014;5:5002.
[121] Liang J, Sun ZH, Li F, et al. Carbon materials for Li-S batteries: functional evolution and performance improvement. Energy Storage Mater 2016;2:76–106.
[122] Sun H, Xu GL, Xu YF, et al. A composite material of uniformly dispersed sulfur on reduced graphene oxide: aqueous one-pot synthesis, characterization and excellent performance as the cathode in rechargeable lithium-sulfur batteries. Nano Res 2012;5:726–38.
[123] Qiu Y, Li W, Zhao W, et al. High-rate, ultralong cycle-life lithium/sulfur batteries enabled by nitrogen-doped graphene. Nano Lett 2014;14:4821–7.
[124] Zu C, Manthiram A. Hydroxylated graphene-sulfur nanocomposites for high-rate lithium-sulfur batteries. Adv Energy Mater 2013;3:1008–12.
[125] Li N, Zheng M, Lu H, et al. High-rate lithium-sulfur batteries promoted by reduced graphene oxide coating. Chem Commun 2012;48:4106–8.
[126] Xa Chen, Xiao Z, Ning X, et al. Sulfur-impregnated, sandwich-type, hybrid carbon nanosheets with hierarchical porous structure for high-performance lithium-sulfur batteries. Adv Energy Mater 2014;4:1301988.

[127] Dong Y, Liu S, Wang Z, et al. Sulfur-infiltrated graphene-backboned mesoporous carbon nanosheets with a conductive polymer coating for long-life lithium-sulfur batteries. Nanoscale 2015;7:7569–73.
[128] Wang H, Yang Y, Liang Y, et al. Graphene-wrapped sulfur particles as a rechargeable lithium-sulfur battery cathode material with high capacity and cycling stability. Nano Lett 2011;11:2644–7.
[129] Yang X, Zhang L, Zhang F, et al. Sulfur-infiltrated graphene-based layered porous carbon cathodes for high-performance lithium–sulfur batteries. ACS Nano 2014;8:5208–15.
[130] Ding B, Yuan C, Shen L, et al. Chemically tailoring the nanostructure of graphene nanosheets to confine sulfur for high-performance lithium-sulfur batteries. J Mater Chem A 2013;1:1096–101.
[131] Zhao MQ, Zhang Q, Huang JQ, et al. Unstacked double-layer templated graphene for high-rate lithium-sulphur batteries. Nat Commun 2014;5:3410.
[132] Shi JL, Tang C, Peng HJ, et al. 3D mesoporous graphene: CVD self-assembly on porous oxide templates and applications in high-stable Li-S batteries. Small 2015;11:5243–52.
[133] Tang C, Li BQ, Zhang Q, et al. CaO-templated growth of hierarchical porous graphene for high-power lithium-sulfur battery applications. Adv Funct Mater 2016;26:577–85.
[134] Zhou G, Zhao Y, Manthiram A. Dual-confined flexible sulfur cathodes encapsulated in nitrogen-doped double-shelled hollow carbon spheres and wrapped with graphene for Li-S batteries. Adv Energy Mater 2015;5:1402263.
[135] Liu Y, Wang X, Dong Y, et al. Self-assembled sulfur/reduced graphene oxide nanoribbon paper as a free-standing electrode for high performance lithium-sulfur batteries. Chem Commun 2016;52:12825–8.
[136] Xu Y, Bai H, Lu G, et al. Flexible graphene films via the filtration of water-soluble noncovalent functionalized graphene sheets. J Am Chem Soc 2008;130:5856–7.
[137] Chen H, Müller MB, Gilmore KJ, et al. Mechanically strong, electrically conductive, and biocompatible graphene paper. Adv Mater 2008;20:3557–61.
[138] Zhou G, Li L, Wang DW, et al. A flexible sulfur-graphene-polypropylene separator integrated electrode for advanced Li-S batteries. Adv Mater 2015;27:641–7.
[139] Shaibani M, Akbari A, Sheath P, et al. Suppressed polysulfide crossover in Li-S batteries through a high-flux graphene oxide membrane supported on a sulfur cathode. ACS Nano 2016;10:7768–79.
[140] Xiao Z, Yang Z, Wang L, et al. A lightweight TiO_2/graphene interlayer, applied as a highly effective polysulfide absorbent for fast, long-life lithium-sulfur batteries. Adv Mater 2015;27:2891–8.
[141] Bai S, Liu X, Zhu K, et al. Metal-organic framework-based separator for lithium–sulfur batteries. Nat Energy 2016;1:16094.
[142] Wang L, Yang Z, Nie H, et al. A lightweight multifunctional interlayer of sulfur-nitrogen dual-doped graphene for ultrafast, long-life lithium-sulfur batteries. J Mater Chem A 2016;4:15343–52.
[143] Peng HJ, Wang DW, Huang JQ, et al. Janus separator of polypropylene-supported cellular graphene framework for sulfur cathodes with high utilization in lithium-sulfur batteries. Adv Sci 2016;3:1500268.
[144] Wu F, Qian J, Chen R, et al. Light-weight functional layer on separator as polysulfide immobilizers to enhance cycling stability for lithium-sulfur batteries. J Mater Chem A 2016;4:17033–41.
[145] Zhuang TZ, Huang JQ, Peng HJ, et al. Rational integration of polypropylene/graphene oxide/nafion as ternary-layered separator to retard the shuttle of polysulfides for lithium-sulfur batteries. Small 2016;12:381–9.
[146] Bai S, Zhu K, Wu S, et al. A long-life lithium-sulphur battery by integrating zinc-organic framework based separator. J Mater Chem A 2016;4:16812–7.
[147] Zhou G, Pei S, Li L, et al. A graphene-pure-sulfur sandwich structure for ultrafast, long-life lithium-sulfur batteries. Adv Mater 2014;26:625–31.
[148] Hu G, Xu C, Sun Z, et al. 3D graphene-foam-reduced-graphene-oxide hybrid nested hierarchical networks for high-performance Li-S batteries. Adv Mater 2016;28:1603–9.
[149] Zhou G, Li L, Ma C, et al. A graphene foam electrode with high sulfur loading for flexible and high energy Li-S batteries. Nano Energy 2015;11:356–65.
[150] Fang R, Zhao S, Pei S, et al. Toward more reliable lithium-sulfur batteries: an all-graphene cathode structure. ACS Nano 2016;10:8676–82.
[151] Lin D, Liu Y, Liang Z, et al. Layered reduced graphene oxide with nanoscale interlayer gaps as a stable host for lithium metal anodes. Nat Nanotechnol 2016;11:626–32.
[152] Zhang R, Cheng XB, Zhao CZ, et al. Conductive nanostructured scaffolds render low local current density to inhibit lithium dendrite growth. Adv Mater 2016;28:2155–62.
[153] Mukherjee R, Thomas AV, Datta D, et al. Defect-induced plating of lithium metal within porous graphene networks. Nat Commun 2014;5:3710.
[154] Cai G, Darmawan P, Cui M, et al. Highly stable transparent conductive silver grid/PEDOT:PSS electrodes for integrated bifunctional flexible electrochromic supercapacitors. Adv Energy Mater 2016;6:1501882.
[155] Zhao Y, Zhang Y, Sun H, et al. A self-healing aqueous lithium-ion battery. Angew Chem Int Ed 2016;55:14384–8.
[156] Shan XY, Wang Y, Wang DW, et al. A smart self-regenerative lithium ion supercapacitor with a real-time safety monitor. Energy Storage Mater 2015;1:146–51.
[157] Pan S, Ren J, Fang X, et al. Integration: an effective strategy to develop multifunctional energy storage devices. Adv Energy Mater 2016;6:1501867.